



Integrated stratigraphy of Pliensbachian and Toarcian strata from the northern Neuquén Basin, Argentina

Marisa S. Storm^{*1, 2, 3}, Stephen P. Hesselbo^{3, 4}, Hugh C. Jenkyns³,
Micha Ruhl^{3, 5}, Aisha H. Al-Suwaidi⁶, Lawrence M. E. Percival^{7, 8},
Tamsin A. Mather³, Susana E. Damborenea⁹, Miguel O. Manceñido⁹
and Alberto C. Riccardi⁹

With 7 figures

Abstract. The Toarcian Oceanic Anoxic Event (T-OAE, ~183 Ma) was marked by globally recognized environmental perturbations, most notably disturbances to the global carbon cycle and climate. To date, geochemical records providing information about the T-OAE have been largely generated from the warm temperate climate zone of the NW European realm. Coeval geochemical records from the Southern Hemisphere, providing a more global perspective on palaeoenvironmental changes associated with the T-OAE, are comparatively scarce. In this study, we present a biostratigraphically calibrated litho- and chemostratigraphic record of Lower Jurassic strata from the northern Neuquén Basin, Argentina, covering the Upper Pliensbachian and Toarcian upper *tenuicostatum* to lower *Dumortieria* Andean ammonite zones, equivalent to the uppermost *tenuicostatum* to *pseudoradiosa* European standard zones. The integrated stratigraphic data re-define the stratigraphic position of the Andean *tenuicostatum*–*D. hoelderi* ammonite Zone boundary and support near-synchronicity of this horizon with the *tenuicostatum*–*serpentinum* zonal boundary in NW Europe. The stratigraphic interval recording the negative carbon-isotope excursion associated with the T-OAE appears massively expanded and organic lean in contrast to the coeval organic-rich deposits in other parts of the Neuquén Basin and in European sections. At Las Overas, persistent sedimentary organic-matter enrichment was limited to brief intervals of black-shale deposition, possibly coinciding with reduced sedimentary organic matter dilution. Depositional rates and inorganic redox proxies suggest that the development of oxygen-depleted conditions may have been disrupted by the interplay between basin subsidence, sedimentation rate, relative sea-level change, depositional setting and deep-water currents.

Keywords. Toarcian, Toarcian oceanic anoxic event, Neuquén Basin, chemostratigraphy, biostratigraphy, organic-matter preservation

Authors' addresses:

- ¹ Department of Marine Microbiology and Biogeochemistry, NIOZ Royal Netherlands Institute for Sea Research, P.O. Box 59, 1790AB Den Burg, Netherlands
- ² Netherlands Earth Systems Science Centre (NESSC), Netherlands
- ³ Department of Earth Sciences, University of Oxford, South Parks Road, OX1 3AN, Oxford, UK
- ⁴ Camborne School of Mines, Department of Earth and Environmental Sciences, University of Exeter, Penryn Campus, Penryn, Cornwall TR10 9FE, UK
- ⁵ Department of Geology, Trinity College Dublin, The University of Dublin, College Green, Dublin 2, Dublin, Ireland
- ⁶ Department of Earth Sciences, Khalifa University of Science and Technology, PO Box 127788, Abu Dhabi, United Arab Emirates
- ⁷ Archaeology, Environmental Changes and Geo-Chemistry, Vrije Universiteit Brussel, Pleinlaan 2, 1050 Brussels, Belgium
- ⁸ Department of Earth Sciences, Faculty of Science, Vrije Universiteit Amsterdam, De Boelelaan 1085, 1081 HV Amsterdam, Netherlands
- ⁹ Departamento Paleontología Invertebrados, Museo de Ciencias Naturales La Plata, Paseo del Bosque s/n, 1900 La Plata, Argentina

* Corresponding author: marisa.storm@nioz.nl

1. Introduction

The sedimentary record of the Lower Toarcian *tenuicostatum* and *serpentinum* European ammonite standard zones and their global equivalents is marked by geochemical signatures of severe climatic, environmental, and oceanographic change associated with the Toarcian Oceanic Anoxic Event (T-OAE; Jenkyns & Clayton 1986, Jenkyns 1988, 2010; Bailey et al. 2003, Dera et al. 2011, Suan et al. 2011, Korte et al. 2015, Remírez & Algeo 2020, Kemp et al. 2022, Gambacorta et al. 2024). Initially recognized by the geographically widespread preservation of coevally deposited organic-rich sediments, the diagnostic interval of the T-OAE is more robustly distinguished stratigraphically by a negative carbon-isotope ($\delta^{13}\text{C}$) excursion (nCIE) punctuating a broader overarching positive shift in $\delta^{13}\text{C}$ (Jenkyns & Clayton 1997, Jenkyns 2003, Kemp et al. 2005, 2020; Xu et al. 2018b, Erba et al. 2022). This nCIE is recorded in organic and inorganic substrates in marine, lacustrine and terrestrial realms globally, consistent with a causal link between the T-OAE and the increased release of isotopically light carbon into the ocean–atmosphere carbon reservoir (Jenkyns 1988, 2010; Hesselbo et al. 2000, 2007; Xu et al. 2017). The exact source(s) of isotopically light carbon remain debated, but likely included volcanogenic and/or bio- and/or thermogenic carbon dioxide and methane (e.g., Hesselbo et al. 2000, McElwain et al. 2005, Svensen et al. 2007, Heimdal et al. 2021). Radioisotopic and magnetostratigraphic dating of igneous rocks from the Karoo-Ferrar Large Igneous Province (LIP) imply that increased volcanic activity of the LIP coincided with the onset of the T-OAE (e.g., Burgess et al. 2015, Xu et al. 2018a, Ware et al. 2023). Enriched sedimentary mercury concentrations in records of the T-OAE have been used as further support of this temporal relationship (e.g., Percival et al. 2015, Fantasia et al. 2018, Ruhl et al. 2022, Fendley et al. 2024). The broad overarching positive shift in $\delta^{13}\text{C}$ is ascribed to the extensive sedimentary drawdown of isotopically light organic matter, provoked by the geographically widespread development of anoxic/euxinic conditions during the Early Toarcian (Jenkyns 2010, Dickson et al. 2017, Them et al. 2018). Large-scale organic-carbon burial during the T-OAE is known from widely distributed shelf-sea settings, deeper marine pelagic basins, and lakes (e.g., Jenkyns 1988, 2010; Gröcke et al. 2011, Xu et al. 2017, Ikeda et al. 2018, Liu et al. 2020, Filatova et al. 2022, Kemp et al. 2022). However, a growing number of age-

equivalent organic-lean records from low-mid latitude southern Iberia and northern and south-western Gondwana (e.g., Bodin et al. 2010, Fantasia et al. 2018, 2019; Silva et al. 2021a) demonstrate differential organic-matter preservation patterns during and around the time of the T-OAE (see overview by Kemp et al. 2022, Ruebsam & Schwark 2024). The scarcity of stratigraphically expanded, and biostratigraphically well-calibrated high-resolution geochemical records from outside the well-studied NW European realm hampers a holistic understanding of the global environmental responses during the T-OAE.

The Neuquén Basin in Argentina offers the possibility for integrated stratigraphic studies on Lower Jurassic sediments deposited within a Southern Hemisphere sedimentary basin. Previous chemostratigraphic studies of the Lower Toarcian strata here have proven the geochemical expression of the T-OAE in the marine sedimentary record of the Neuquén Basin (Al-Suwaidi et al. 2010, 2016, 2022). The correlation between the European and Andean ammonite zonation (Riccardi 2008) allows a comparison with the chemostratigraphic records from NW Europe.

Here, we present a new high-resolution integrated record from the Lower Jurassic Upper Pliensbachian and Toarcian strata of the Mendoza region, Neuquén Basin, Argentina, combining bio-, litho- and chemostratigraphic data. The data extend the previous records from this area to stratigraphically lower and higher levels, and resolve stratigraphic uncertainties within the previous studies, including redefinition of the *tenuicostatum*–*D. hoelderi* ammonite zonal boundary locally. Combined bio- and chemostratigraphic context allows identification of the negative carbon-isotope excursion associated with the T-OAE. The chemostratigraphic correlation also illustrates the near-synchronicity of the Andean and NW European ammonite-based biostratigraphy with respect to the *tenuicostatum*–*D. hoelderi* and *tenuicostatum*–*serpentinum* zonal boundaries. Changes in organic-matter accumulation and preservation within the succession can be linked to local and/or regional depositional factors.

2. Geological setting

The Neuquén Basin developed as part of a larger Mesozoic back-arc system, the Andean Basin, which formed on the western margin of Gondwana, roughly parallel to the modern-day Andes of Argentina, Chile and northern Peru (Fig. 1A; Vicente 2005). Driven by plate-tectonic movement, the Neuquén Basin migrated

between 56° and 25°S in the Early Jurassic (Franzese et al. 2003, Iglesia-Llanos et al. 2006). Today located in west-central Argentina on the eastern side of the Andes, the Neuquén Basin covers an area of ~120,000 km² and comprises up to ~6 km of Upper Triassic to Eocene sedimentary fill (Legarreta & Uliana 1996, Howell et al. 2005).

The basin originated in the Late Triassic, when the area was subject to continental extension related to the collapse of the Gondwana orogen (Franzese & Spallietti 2001). The rifting generated a series of unconnected N–S-trending half-grabens (Vergani et al. 1995, Legarreta & Uliana 1996, Franzese & Spallietti 2001). The pre-Andean volcanic arc (Chilean Coastal Cordillera) to the west of the young basin acted as a barrier to the Panthalassa (palaeo-Pacific) Ocean (Fig. 1B; Vicente 2005, Franzese et al. 2006). Marine sedimentation started in the Late Triassic/Early Jurassic in the northern Neuquén Basin, when a narrow marine corridor, the Curepto Strait, developed and connected the basin to the Panthalassa Ocean (Fig. 1B, Legarreta & Uliana 1996, Vicente 2005).

During the Late Pliensbachian and Toarcian, the Neuquén Seaway expanded southward into the dispersed depocentres that had developed during the pre-rift phase (Vicente 2005). The development of an active subduction zone on the western margin of Gondwana during the Early Jurassic–Early Cretaceous was associated with, and the root cause of, the evolution of the magmatic arc and back-arc subsidence within the Neuquén Basin (syn- and post-rift phase), interrupted by episodic basin inversion (Vergani et al. 1995, Franzese & Spallietti 2001). Thermal subsidence and regional back-arc extension led to marine transgression and general deepening during the Late Pliensbachian and Early Toarcian, and successively deeper marine facies were deposited as part of the Cuyo Group (Legarreta & Uliana 1996, Vicente 2005). Transgressive–regressive cycles were driven by changes in the subsidence rate, localized episodic uplift, as well as eustatic sea-level oscillations (Howell et al. 2005). During the marine phase, siliciclastic sediments were supplied from the cratonic eastern margin of the basin, forming a transgressive siliciclastic platform, whereas volcaniclastics, sourced from the Chilean Coastal Cordillera, entered the basin on the western margin (Vicente 2005).

The study area is located in the Valenciana depocentre in the northern Neuquén Basin (Fig. 1B). The Lower Jurassic sediments are of marine and marginal marine origin and form part of the lower Cuyo Group.

Palaeogeographically, the study area was located proximal to the Curepto Strait that fed seawater from the Panthalassa Ocean into the Neuquén Basin (Fig. 1B). Sinemurian to Aalenian strata are represented by the Puesto Araya and Tres Esquinas Formations, which are stratigraphically equivalent to the Los Molles Formation of the southern Neuquén Basin (Fig. 2; Gulisano & Gutiérrez-Pleimling 1995). The Sinemurian to Upper Pliensbachian Puesto Araya Formation is interpreted to record a gradual transition from inner- to outer-shelf facies of a near-shore sedimentary environment, whereas the Tres Esquinas Formation comprises outer-shelf to basin deposits (Gulisano & Gutiérrez-Pleimling 1995, Leanza et al. 2013).

3. Materials and methods

3.1 Materials

The field area (location 3 in Fig. 1B) is situated in the northern Neuquén Basin, Mendoza Province, ~30 km west of the city of Malargüe (35°25'49" S, 69°53'40" W, Fig. 1C). Six stratigraphic sections were logged along, and east of, the Arroyo Serrucho creek and the Las Overas creek (Fig. 1C–E). Bulk-rock samples were collected at 10 to 100 cm spacing, depending on exposure and lithologies. In all sections, ammonites, bivalves and brachiopods were collected wherever found *in situ*. Fossils collected *ex situ* are labelled accordingly (Supplementary Fig. 1, 3–4)

3.2 Rock-Eval analysis

Bulk-rock samples were powdered at the Department of Earth Sciences, University of Oxford, using a rock hammer, a Fritsch mortar grinder, and agate mortar. Rock-Eval analysis was performed on bulk-rock samples on a Rock-Eval 6 Standard Analyzer unit from Vinci Technologies, including a pyrolysis and oxidation oven (Behar et al. 2001). For each sample, 50–100 mg of homogenized, powdered bulk-rock were analysed to determine the content of total organic carbon (TOC, wt%) and mineral carbon or total inorganic carbon (TIC, wt%), as well as the Hydrogen Index (HI, mg HC/g TOC), Oxygen Index (OI, mg CO₂/g TOC) and T_{max} (°C) values. The standard deviation (SD) on TOC and HI measurements of the in-house SAB134 (Blue Lias organic-rich marl) standard was 0.11 wt% and ±29.95 mg HC/g TOC, respectively. The SD for T_{max}, OI and TIC measurements was 1.9 °C, 2.8 mg CO₂/g TOC and 0.25 wt%, respectively.

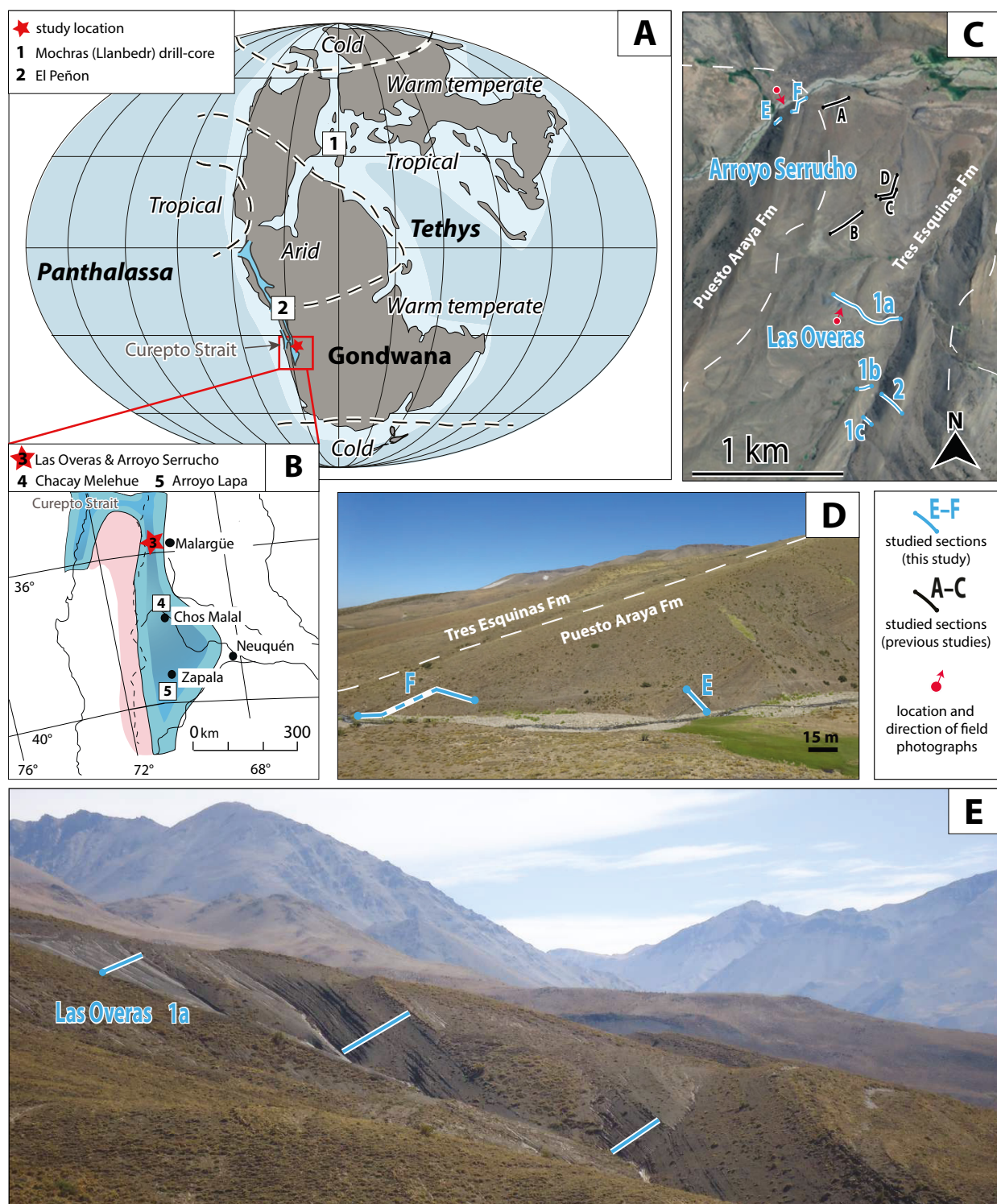


Fig. 1. Toarcian palaeogeography, study locations and field photographs. **A:** Toarcian palaeogeography (after Blakey 2007) indicating the approximate location of the Andean Basin (modified from Vicente 2005) and position of Early Jurassic palaeoclimatic belts after Scotese (2013). Location of the Neuquén Basin indicated by the red square. Lower Jurassic sections outside the Neuquén Basin discussed in the main text labeled with numbers. **B:** Neuquén Basin during the Early Jurassic (after Vicente 2005) with present-day coordinates. Relative water depth indicated by different colours (darker blue = deeper water). Approximate location of the Chilean Coastal Cordillera marked in red. Stratigraphic sections discussed in text labelled with numbers. **C:** Satellite image (Google Earth, December, 2022) showing sections previously studied by Al-Suwaidi et al. (2016) (Arroyo Serrucho A, B, C) and Mazzini et al. (2010) (Arroyo Serrucho D) in the study location, as well as sections examined in this study (Arroyo Serrucho E and F, Las Overas 1a, b, c and Las Overas 2). The white dashed lines mark the approximate lower and upper boundaries of the Tres Esquinas Fm, modified from Gulisano & Gutiérrez-Pleimling (1995). **D:** Field photograph showing the upper Puesto Araya Fm. The location and direction from which this photograph was taken are indicated in Fig. 1C. Locations of the study sections Arroyo Serrucho E and F are marked in blue. The approximate position between the Puesto Araya Fm and Tres Esquinas Fm is marked as a white dashed line. **E:** Field photograph showing a view onto the strata of the lower Las Overas section (upper *tenuicostatum* Zone and lower *hoelderi* Zone) of the lower Tres Esquinas Fm. The location and direction the photograph was taken from are indicated in Fig. 1C.

The long-term average TOC of the international reference standard IFP 160000 is 3.27 wt%, with a standard deviation of 0.05 wt%.

3.3 Organic carbon-isotope analysis

About 1–2 g of homogenized powdered bulk-rock sample were treated with ~30 ml of 3 M HCl in a warm water bath (~80 °C) for about 24 hours to remove calcium carbonate in preparation for $\delta^{13}\text{C}$ analysis of the TOC ($\delta^{13}\text{C}_{\text{TOC}}$). Samples were then centrifuged and the HCl decanted. Carbonate-rich samples were treated with HCl a second time. The carbonate-free samples were then rinsed with deionized water until a neutral pH was reached. The samples were centrifuged and the remaining water was decanted before samples were dried in an oven overnight at ~40 °C. Dried, decarbonated sample powders were weighed into 8 × 6 mm tin capsules (~10 mg of sample).

The $\delta^{13}\text{C}_{\text{TOC}}$ analyses were performed on a Thermo Finnigan MAT 253 mass spectrometer at the Stable Isotope Geochemistry Laboratory of the Open University (Milton Keynes, UK), for a total of 576 samples. The measured $\delta^{13}\text{C}$ values were corrected using a three-point calibration with the in-house standards: IAEA-CH-6 sucrose, NIST8573 glutamic acid and IR-041 alanine. The $\delta^{13}\text{C}$ values are reported in ‰ relative to the VPDB standard. Replicate analysis of the standard showed a precision of $\pm <0.1\text{‰}$ (1 SD).

3.4 Elemental concentrations

Elemental concentrations of silicon (Si), aluminium (Al), sulphur (S), titanium (Ti), zirconium (Zr), vana-

dium (V), nickel (Ni) and molybdenum (Mo) were obtained by hand-held X-ray fluorescence (HH-XRF) analysis, performed on 629 bulk-rock samples. A hand-held Olympus Innov-X Delta Premium DP6000C XRF Alloy Analyzer adjusted in a stand was used on the flat surface of bulk-rock samples. The analyzer utilised a 4W X-ray tube and a large-area Silicon Drift Detector. X-ray absorption spectra were recorded in scanning mode from 3 to 40 keV and absorption peaks were automatically identified using the Innov-X “soil mode” software. Scanning time was set to 60 seconds for each light and heavy element. All analyses were run in the Geochem Mode (DS-6000) and manufacturer-delivered standards were used for calibration. The standard NIST 2710a was repeatedly measured for the analysis, with average values as follows: **Si** (23.9 ± 0.5 wt%), **Al** (5.6 ± 0.1 wt%), **S** (1.78 ± 0.035 wt%), **Ti** (0.29 ± 0.007 wt%), **Zr** (210 ± 30 ppm), **V** (290 ± 23 ppm), **Ni** (15 ± 3 ppm), **Mo** (5 ± 1 ppb).

3.5 Sedimentary mercury

Sedimentary mercury (Hg) analyses were performed on 72 samples, with only samples with $\text{TOC} \geq 0.5$ wt% selected for interpretation following the recommendations of previous studies and reflecting the important role of TOC as a Hg host phase (Grasby et al. 2016). The analysis was performed using a Lumex RA-915 Portable Mercury Analyzer with PYRO-915 Pyrolyzer, as described by Bin et al. (2001). Powdered sample (~100 mg) was weighed into a glass measuring boat and its precise mass determined. The sample was then placed into the pyrolyzer (set at Mode 1), which

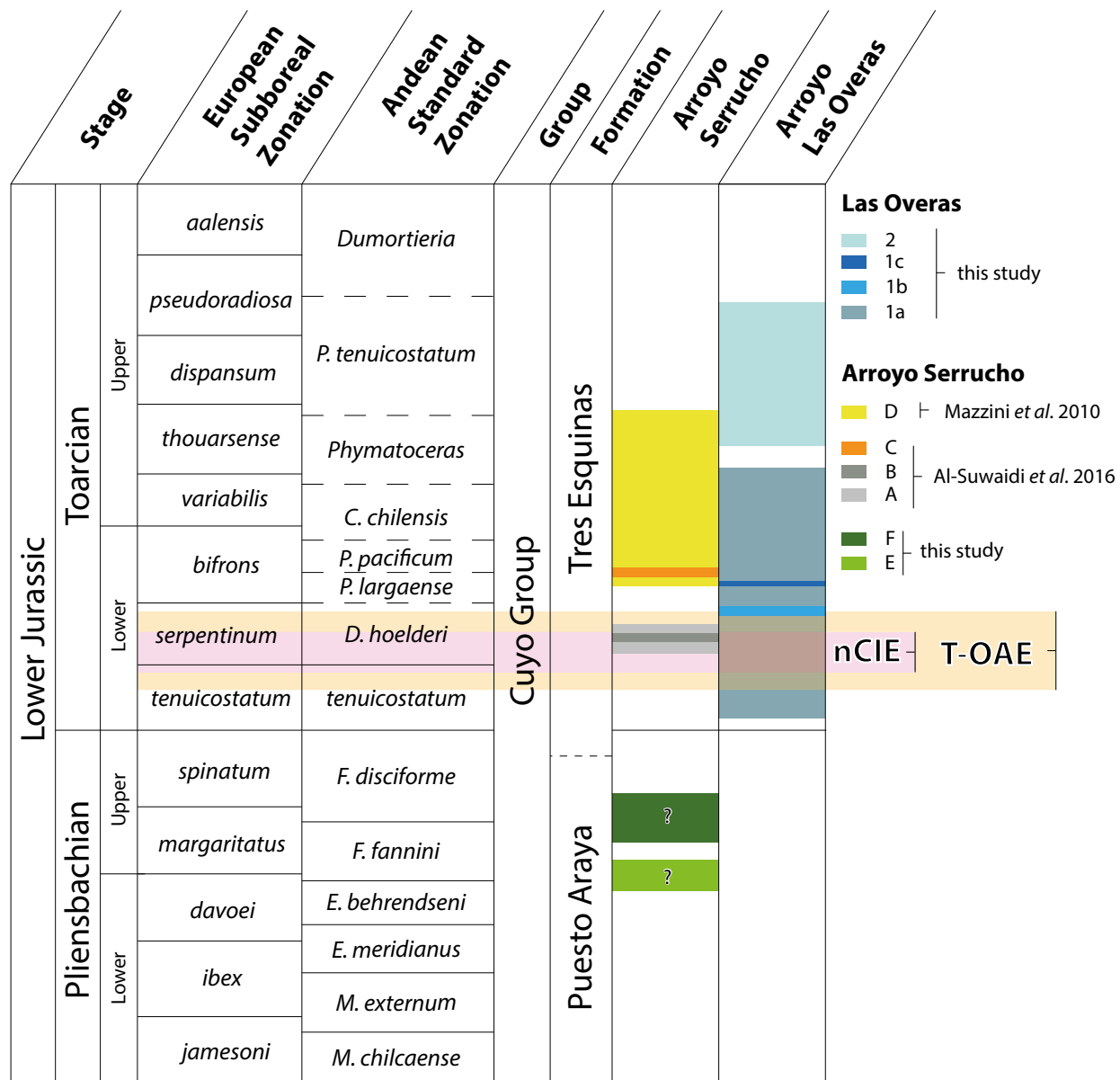


Fig. 2. Table showing the epoch, standard NW European biozones (after [Page 2003](#)), Andean ammonite zonation (after [Riccardi 2008](#)), group and formations of the studied strata, and overview of the stratigraphic position of sections examined in this and previous studies ([Mazzini et al. 2010](#), [Al-Suwaidi et al. 2016](#)). Figure modified after [Al-Suwaidi et al. \(2016\)](#). Approximate stratigraphic position of the T-OAE interval (orange), and the negative carbon-isotope excursion associated with the T-OAE (nCIE, pink) follows the definition of [Gambacorta et al. \(2024\)](#).

heated it to 700 °C to volatilize the Hg from the sediment. The resulting gas was analysed by atomic absorption spectroscopy to detect and calculate the elemental Hg concentration. As a standard, variable-mass (between 10 and 90 mg) samples of peat (NIMT/UOE/FM/001 – Inorganic Elements in Peat) with a known Hg concentration of 169 ± 7 ng/g were used for calibration of the instrument. This calibration was checked

daily prior to the analysis of rock samples, using five variable-mass peat samples. Additionally, a 50 ± 2 mg sample of the peat standard was analysed after approximately every tenth measurement to ensure analytical accuracy, and each sample analysed at least twice to check reproducibility, which was typically within 10%.

4. Results

4.1 Lithofacies

Arroyo Serrucho section E: The stratigraphically lowest section examined is located along the south side of the Serrucho stream (base: $35^{\circ}25'54.6''$ S, $69^{\circ}54'25.2''$ W, Fig. 1C). The section covers 15.7 m of strata and comprises calcareous and fossiliferous, rusty-weathering mud-, silt- and sandstone, with some intercalated volcaniclastic beds (Fig. 3, S1). The individual beds are 10 to 60 cm thick and show fining-upwards trends with shell debris particularly common in the upper few centimetres. The rich fossil fauna includes bivalves, some of which are in life position, brachiopods and crinoids; burrows (*Thalassinoides* and *Lapispira bispiralis*) are common. Ammonites were also recovered from these strata.

Arroyo Serrucho section F: The section is also located along the south side of the Serrucho riverbed (base: $35^{\circ}25'53.6''$ S, $69^{\circ}54'20.8''$ W, 70 samples) and covers 30.2 m of stratigraphy (Fig. 1C, 3, S1). The base of the section lies stratigraphically approximately 50 m above the top of Arroyo Serrucho E. Due to vegetation cover, the stratigraphic interval in between Arroyo Serrucho E and F was not logged or sampled. The lithology of the lower part of section F is similar to that of section E, comprising rusty-weathering calcareous and fossiliferous mud-, silt- and sandstone, with some intercalated volcaniclastic beds. Bivalves occur throughout the section; however, in life position, they are only found at the base of the section. Closer to the top of the succession, the lithology contains an increasing amount of finer grained mudstone and some rusty-weathering beds are locally developed.

The Las Overas 1 composite section is composed of three individual sections. Las Overas Section 1a is the principal section, with overall the best and most continuous exposure in the study area. However, due to the presence of a fault cutting through the succession, missing strata between 60.8 and 70.7 m were instead described and sampled in a gully ~0.5 km to the south, at Las Overas section 1b (Fig. 1C). There, the succession is continuous for several metres both above and below the interval of the unexposed strata in Section 1a, allowing precise and confident correlation and splicing (Fig. 3, S1, S2). Poorly exposed strata within the interval of 83.9 to 85 m of section 1a were instead sampled at Section 1c (Fig. 1C) where strata were well exposed and the unique phosphatic and fossiliferous marker bed (at 85.4 m in Las Overas section 1a) could

be recognized, thereby allowing a precise correlation of the strata.

Las Overas section 1a: The strata crop out along the Las Overas creek, approximately 1.2 km SSE of Arroyo Serrucho F (base: $35^{\circ}26'35.9''$ S, $69^{\circ}54'10.0''$ W). The section covers 135.9 m of stratigraphy (Fig. 1C, and S1) and comprises sediments that are generally finer grained compared to those of the stratigraphically lower Arroyo Serrucho sections E and F. The lower ~35 m of the section comprise medium-grey mudstone, intercalated with laminated, dark-grey mudstone beds of varying thickness from 20 cm to 2.5 m. Between 35 and 80 m, hummocky cross-bedded sandstone beds rich in fossiliferous debris and with erosional bases appear intercalated in the mudstone succession, likely representing tempestites. Red-to pink-weathering nodules and cemented beds appear commonly within the lower ~51 m of the section. The nodules possess characteristics similar to the sandstone beds, including hummocky cross-stratification, and fossil debris concentrated at the base, and could represent diagenetically altered remains of storm deposits.

A phosphate-rich bed occurs between ~85.4 and 86.4 m, containing abundant ammonites and fossil wood fragments. The bed is likely highly condensed and represents a distinct stratigraphic marker. Above 86.5 m, the lithology appears more homogenous, comprising dark-grey silt-rich mudstone with commonly intercalated cross-bedded arenaceous deposits. Ammonites are rare; belemnites occur in the upper part of the section. Volcaniclastic (ash) beds are intercalated through the entire section.

Las Overas section 1b: The base of the section is located at $35^{\circ}27'04''$ S, $69^{\circ}55'01''$ W, and covers 10 m of stratigraphy (Fig. 1C, 3, S1). The basal 2 m of the recorded section are marked by two fossiliferous sandstone and siltstone beds (~40–60 cm), separated by ~60 cm of mudstone. A predominantly dark-grey silty mudstone follows stratigraphically up-section, with intercalated 20–40 cm-thick siltstone and cross-bedded sandstone beds.

Las Overas section 1c: This section is located about 700 m south of Las Overas 1a and approximately 200 m south of Las Overas 1b and covers 1 m of stratigraphy ($35^{\circ}27'08''$ S, $69^{\circ}54'02''$ W; Fig. 1C, S1). The succession comprises dark-grey silty mudstone.

Section Las Overas 1a together with the sections 1b and 1c are in the following discussed as the Las Overas 1 composite section.

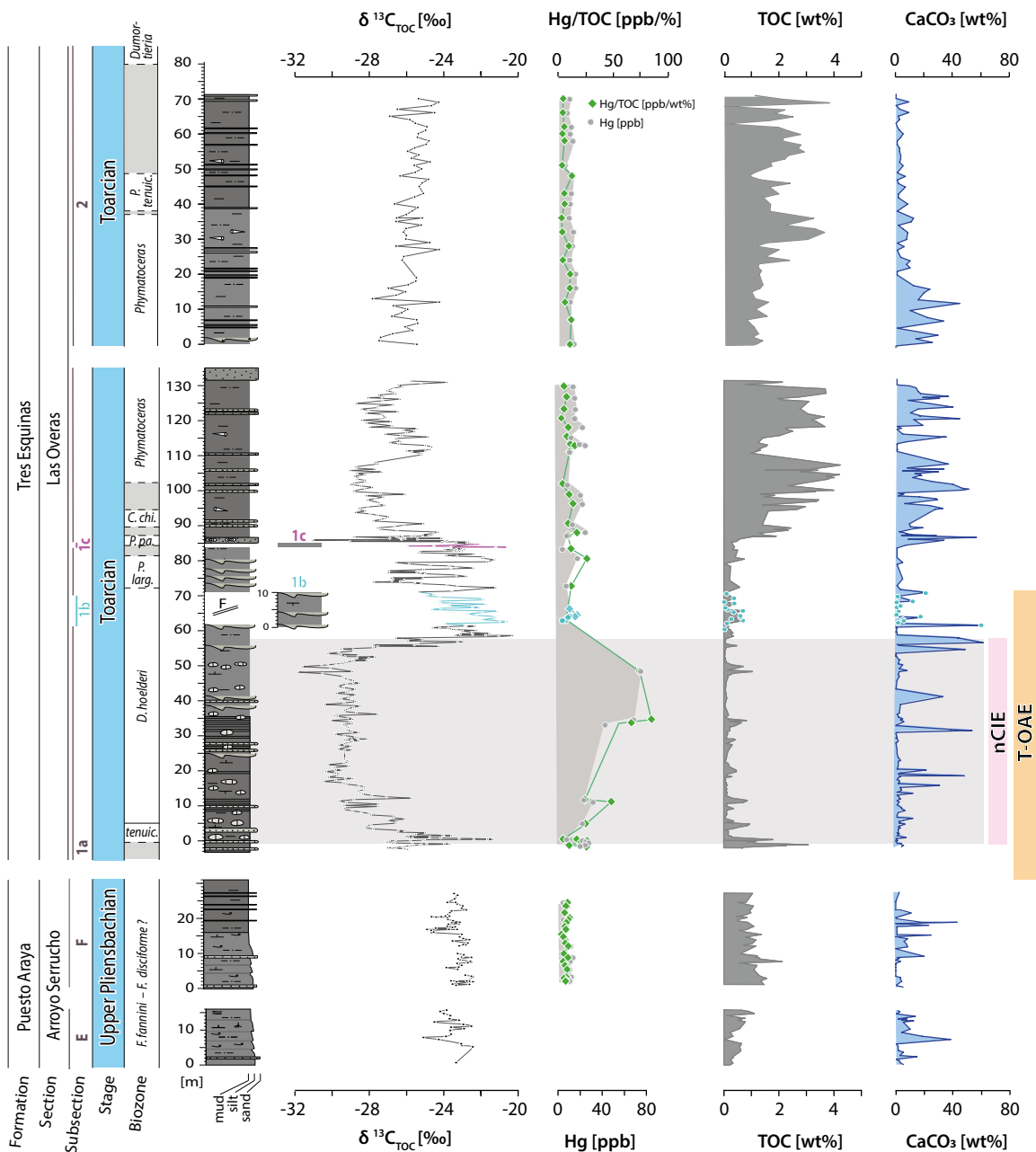


Fig. 3. Lithology, ammonite zonation and chemostratigraphic record ($\delta^{13}\text{C}_{\text{TOC}}$, TOC, CaCO_3 , Hg and Hg/TOC) of the studied sections. Approximate stratigraphic position of the T-OAE and nCIE intervals marked in orange, and grey/pink, respectively. Stratigraphic gaps between individual sections not to scale. Las Overas 1b and 1c are plotted at the stratigraphic position relative to Las Overas 1a. The data generated from samples taken from section 1b are plotted in light blue. Data obtained from Las Overas 1c samples are shown in lilac.

Las Overas section 2: The base of Las Overas section 2 is located approximately 100 m southeast of Las Overas 1b, on the eastern side of the valley (35°27'05.5" S, 69°53'58.8" W; Fig. 1C). Las Overas section 2 continues stratigraphically above the Las Overas 1 composite section. No stratigraphic markers

were found that would suggest a stratigraphic overlap between the two sections. The thickness of strata not exposed between the two sections could not be determined accurately due to the morphology of the field area. The section covers 73 m of stratigraphy (Fig. 3, S1) and comprises a homogenous lithology of silt-rich

mudstone, intercalated by 5–10 cm-thick dark-grey cemented mudstone beds, as well as cross-bedded sandstone beds. Belemnites are common here.

4.2 Litho- and biostratigraphy

The lithological observations and invertebrate faunas of Arroyo Serrucho section E (Fig. 3, S1, S3) correspond with the previous descriptions of the oxygenated near-shore to inner-shelf deposits of the Upper Pliensbachian upper Puesto Araya Formation ([Gulisano & Gutiérrez-Pleimling 1995](#)). The bivalve faunas (described by [Damborenea 1987, 2002](#); [Echevarría et al. 2021](#)) are diverse and belong to a variety of near-shore environments. The occurrence of the bivalve *Radulonectites sosneadoensis* (Weaver) at 15.5 m in section E and near the base of section F (Fig. S3) indicates the *R. sosneadoensis* bivalve Assemblage Zone of Late Pliensbachian age ([Damborenea 2002](#)); in addition, the widespread presence of *Rhynchonelloidea cuyana* Manceñido throughout section F and the entire section E is indicative of the Late Pliensbachian (to earliest Toarcian) *R. cuyana* brachiopod Assemblage Zone ([Manceñido 1990](#)). The occurrence of the trace fossil *Lapispira bispiralis* throughout Arroyo Serrucho section E and up to ~24 m in Arroyo Serrucho F is also consistent with a depositional environment in the offshore–shoreface transition Zone ([Lanés et al. 2007](#)). The relative increase of fine-grained sediments (mudstone) in the Arroyo Serrucho section F compared to the underlying coarser-grained Arroyo Serrucho E reflects gradual deepening, in accordance with syn-sedimentary basin subsidence and sea-level rise during the Late Pliensbachian–Early Toarcian transition.

In both Arroyo Serrucho sections E and F ammonite records are scanty. *Austromorphites behrendseni* was recovered from sediments approximately 40 m below the base of Arroyo Serrucho section E, indicating the *A. behrendseni* Zone for the underlying strata (Plate S1A). *Fanninoceras?* sp. has been found close to Arroyo Serrucho section E, in strata that could laterally be traced to the basal beds of the section. Based on these observations, the strata covered by Arroyo Serrucho section E and the suprajacent section F are tentatively assigned to the *F. fannini*–*F. disciforme* ammonite Zones.

The lithologies of the Las Overas 1 composite and Las Overas 2 sections correspond to descriptions of the Tres Esquinas Formation, comprising dark-grey calcareous, partly laminated silt- and claystones and intercalated arenaceous beds in the lower section,

likely representing frequent storm deposits. Gravity flows, which appear more commonly from the stratigraphic marker bed at 85.4 m stratigraphically upwards, suggest a gradually deepening succession from inner-shelf to less-oxygenated outer-shelf deposits.

The sharp lithological contact dividing the Puesto Araya from the overlying Tres Esquinas Formation described by [Gulisano & Gutiérrez-Pleimling \(1995\)](#) has not been observed in either Arroyo Serrucho F or the Las Overas 1 composite section, suggesting that the boundary between the two formations (stratigraphically positioned in the Upper Pliensbachian mid-*spinatum* Zone) is likely located in the exposure gap between Arroyo Serrucho F and the Las Overas 1 composite section.

The ammonite biostratigraphy presented in this study (Fig. S1, S4, Plate S1A–B) places the *tenuicostatum*–*D. hoelderi* boundary within the lower Las Overas 1 composite section (at 5 m) based on the lowest occurrence (LwO) of *Dactylioceras (Orthodactylites) cf. hoelderi* (Hillebrandt & Schmidt-Effing). The *D. hoelderi*–*P. largaense* zonal boundary is placed at 72.1 m based on the LwO of *Harpoceras cf. falciferum* (J. Sowerby). The *P. largaense*–*P. pacificum* zonal boundary is placed at 84.3 m based on the LwO of *Harpoceras cf. subplanatum* (Oppel) and *Peronoceras cf. verticosum* Buckman. The LwO of *Collina cf. chilensis* Hillebrandt & Schmidt-Effing at 89.7 m marks the *P. pacificum*–*C. chilensis* zonal boundary. At 100.23 m, the LwO of *Phymatoceras cf. copiapense* (Möricker) defines the *C. chilensis*–*Phymatoceras* zonal boundary.

At Las Overas section 2, the occurrence of *Phymatoceras cf. copiapense* (Möricker) at 37 m indicates the *Phymatoceras* Zone. The *Phymatoceras*–*P. tenuicostatum* zonal boundary is placed at 38 m, based on the LwO of *Phlyseogrammoceras cf. tenuicostatum* (Jaworski). The LwO of *Pleydellia cf. fluitans* (Dumontier) marks the *P. tenuicostatum*–*Dumorteria* zonal boundary at approximately 80 m (after [Riccardi 2008](#), Fig. S1, S4).

Other complementary data of biostratigraphical significance (Fig. S4) include the occurrence of brachiopods indicative of the Late Pliensbachian to Early Toarcian *Rhynchonelloidea cuyana* Assemblage Zone between –1.15 m and 1.80 m (Las Overas 1 composite section), and those representative of the Early Toarcian *Rhynchonelloidea lamberti* Assemblage Zone between 8.10 m and 80.40 m ([Manceñido 1990](#)). Among bivalves, those belonging to the *Posidonotis cancellata* Assemblage Zone occur from –1.15 up to 6 m;

whilst those of the *Parvamussium pumilum* Assemblage Zone are recorded from 35.40 m to 77.5 m.

4.3 Organic carbon-isotope record

The $\delta^{13}\text{C}_{\text{TOC}}$ values recorded in the strata of Arroyo Serrucho E and F range between -22.4 and $-25.1\text{\textperthousand}$. Two minor negative shifts of 2 and $2.5\text{\textperthousand}$ are recorded in Serrucho E between 5.2–10.4 m and 11.1–13.2 m, respectively. Similarly, two prominent negative shifts of $\sim 2\text{\textperthousand}$ magnitude are recorded in Arroyo Serrucho F between ~ 13.9 –18.45 m and ~ 18.8 –22.4 m (Fig. 3).

The $\delta^{13}\text{C}_{\text{TOC}}$ values recorded at the Las Overas 1 composite section range between -20.3 and $-31.8\text{\textperthousand}$ (Fig. 3). The strata between 2.6 and 0.3 record an overall trend towards more positive values from -25.9 to $-21.4\text{\textperthousand}$. The stratigraphic interval between 0.3 and 16.9 m is characterized by an overall trend towards lower $\delta^{13}\text{C}_{\text{TOC}}$ values, falling stepwise from $\sim -26.8\text{\textperthousand}$ to $-30.5\text{\textperthousand}$.

Between 16.9 and 45.7 m, $\delta^{13}\text{C}_{\text{TOC}}$ values remain relatively low ($-29.2\text{\textperthousand}$ on average), and include two distinct further negative $\delta^{13}\text{C}_{\text{TOC}}$ shifts, with values decreasing to -31.8 and $-31.6\text{\textperthousand}$ at ~ 48.1 and ~ 49.7 m, respectively. Above the second of these intervals there follows a stepwise shift towards more positive isotopic values, reaching a maximum of $-20.3\text{\textperthousand}$ at 58.6 m. The $\delta^{13}\text{C}_{\text{TOC}}$ record of the suprajacent strata (58.7 to 85.2 m; upper *D. hoelderi* Zone to lower *P. pacificum* Zone) is highly fluctuating around an average value of $-29.9\text{\textperthousand}$. The phosphate-rich marker bed (~ 85.4 –86.4 m; upper *P. pacificum* Zone) is marked by three brief but sharp (single-data-point) negative shifts in $\delta^{13}\text{C}_{\text{TOC}}$, from $-22.7\text{\textperthousand}$ to $\sim -31.0\text{\textperthousand}$ (at 85.4 m, 85.9 m and 86.4 m, respectively). Stratigraphically above these shifts, the $\delta^{13}\text{C}_{\text{TOC}}$ record trends to more positive values ($-24.1\text{\textperthousand}$). Above the marker bed, $\delta^{13}\text{C}_{\text{TOC}}$ values decrease gradually to $-29.1\text{\textperthousand}$ at 105 m (*Phymatoceras* Zone). A positive shift to $-24.7\text{\textperthousand}$ between 110.3 and 112.6 m is followed by another stratigraphically expanded negative shift and subsequent increase of $\delta^{13}\text{C}_{\text{TOC}}$ values, falling to -28.7 at 125 m and increasing to $-23.8\text{\textperthousand}$ at 131 m.

Las Overas section 2 is characterized by a gradual $\sim 3\text{\textperthousand}$ increase in $\delta^{13}\text{C}_{\text{TOC}}$. Values gradually increase, albeit fluctuating, from -27.5 at 1 m to -24.3 at 69 m (upper *Phymatoceras* Zone to upper *P. tenuicostatum* Zone, Fig. 3).

4.4 Maturity of the organic matter

Rock-Eval-generated T_{max} values indicate the overmature nature of the organic matter (T_{max} values between 502 and 578 °C, with an average of 520 °C, see Supplementary Data). T_{max} values obtained from samples with <0.5 wt% TOC yielded unreliable results. Due to the high level of thermal maturity, Hydrogen and Oxygen Indices cannot be interpreted to reflect sedimentary organic-matter sources and are not discussed.

4.5 Total organic carbon (TOC)

The total organic-carbon (TOC) record of Arroyo Serrucho E is marked by a gradual increase in values from below 0.5 wt% at the base to ~ 1 wt% at the top of the section (Fig. 3). Arroyo Serrucho F is characterized by overall slightly higher TOC values (0.9 wt% on average), and a gradual decrease from ~ 1.4 wt% to 0.7 wt% through the section.

At the Las Overas 1 composite section, the strata between ~ 2.6 to 0.2 m (*tenuicostatum* Zone) are characterized by an increase in TOC values from 0.6 to 3 wt% (Fig. 3). The values then decrease in the overlying strata and remain low (0.25 wt% on average) between 0.2 and 86.4 m (*tenuicostatum* Zone to *P. largaense* Zone). Individual stratigraphic intervals of 1–4 m record higher TOC values of up to 1 wt% (Fig. 3).

TOC values increase gradually from ~ 86.4 m upwards following the condensed, phosphate-rich stratigraphic marker bed, reaching ~ 4.2 wt% at 107.3 m (lower *Phymatoceras* Zone). TOC values remain relatively elevated in the upper Las Overas 1 composite section (1–3.6 wt%), with slightly lower values between 110 and 115 m. Las Overas section 2 records TOC values of 1.3 wt% on average throughout the lower 30 m (upper *Phymatoceras* Zone). TOC increases between 30 and 40 m (uppermost *Phymatoceras* Zone to lowermost *P. tenuicostatum* Zone), reaching up to 3.8 wt%, and remains at ~ 2.2 wt% on average throughout the remainder of the section (*P. tenuicostatum* Zone).

4.6 Calcium carbonate content (CaCO_3)

The percentage CaCO_3 was reconstructed from Rock-Eval-analysed total inorganic carbon concentrations (TIC), assuming all mineral carbon occurs as CaCO_3 . Arroyo Serrucho E and F sections are both character-

ized by overall low CaCO_3 concentrations of <10 wt%. Some individual samples, however, record higher CaCO_3 content of up to 40 wt% (Fig. 3).

Las Overas strata are also characterized by overall low CaCO_3 values in the lower 86.5 m (*tenuicostatum* Zone to *P. pacificum* Zone), with values of ~6 wt% on average, although some individual samples show increased CaCO_3 values of up to 59 wt% (Fig. 3). The CaCO_3 content increases in the *P. chilensis* Zone, above the condensed phosphate-rich stratigraphic marker bed, and remains elevated throughout the remainder of the measured section, with average values of 15 wt%, and individual samples with higher values of 30–57 wt%.

CaCO_3 values remain relatively elevated through the lower 20 m of Las Overas section 2 (18 wt% on average throughout the *Phymatoceras* Zone). Values decrease to 4 wt% on average through the upper part of the section.

4.7 Major and trace elements

Elemental Zr, Si and Ti were normalized against Al to account for changes in fine detrital input. Tempestite (redeposited) levels show relatively increased Si/Al, Ti/Al and Zr/Al ratios throughout the section, reflecting higher siliciclastic input, and suggesting a shift to larger grain size associated with these deposits relative to the mudstone facies (Fig. 4A; cf. Calvert & Pedersen 2007). A general shift towards relatively elevated Ti/Al and Zr/Al ratios is recorded between the mid-*hoelderi* Zone to upper *P. largaense* Zone (54–80 m), where coarse-grained storm deposits are common. Si/Al indicates a high variability in siliciclastic input. The onset of this interval coincides with the termination of the nCIE and recovery towards more positive $\delta^{13}\text{C}$ values. The return to lower Ti/Al and Zr/Al ratios and lower variability in siliciclastic input at 80 m coincides with the change in facies towards finer grained and deeper marine sediments.

Redox-sensitive sedimentary Mo concentrations are largely below the HH-XRF detection limit in the lower part of the Las Overas 1 composite section. Some stratigraphically short intervals record sedimentary Mo concentrations (up to 14 ppm; Fig. 4B). One brief interval of increased Mo values is recorded in the upper *tenuicostatum* Zone, where it appears at the same stratigraphic level as a positive shift in $\delta^{13}\text{C}_{\text{TOC}}$ and an enrichment in TOC. The Mo-enriched intervals in the overlying strata are associated with laminated mudstone facies in the lower and mid *D. hoelderi*

Zone. Stratigraphically above the condensed phosphate-rich marker bed in the *P. pacificum* Zone (86.4 m), Mo values are on average well above detection limit, reaching up to 10–40 ppm, suggesting the development of more oxygen-depleted, and at times intermittently euxinic conditions (Mo >25 ppm; Dahl et al. 2013) during deposition of the upper Las Overas 1 composite record. Values of molybdenum normalized to aluminium (Mo/Al), which account for differences in fine detrital input, record the same general trend (Fig. 4B). V- and Ni-abundances record a similar pattern to Mo and Mo/Al. Although the sediment is enriched in Mo and V relative to average shale (Wedepohl 1971) throughout the section, Ni-enrichment is restricted to intervals of relatively elevated Mo and V.

Elemental sulphur values are largely below detection limit. Values of up to 4 wt% correspond principally to stratigraphic intervals of laminated strata in the lower Las Overas 1 composite section, and finer grained lithologies in the upper section (see supplementary data set).

4.8 Sedimentary mercury

Mercury (Hg) levels measured in Arroyo Serrucho and Las Overas strata range between 3.3 and 76 ppb (Fig. 3, 4A). Hg can be found in multiple host phases including organic matter, clay minerals and sulfides (Grasby et al. 2019); consequently, Hg concentrations recorded at the Las Overas 1 composite section are normalized to TOC, elemental sulphur, elemental aluminium and aluminium-normalized silicon (Fig. 4A). TOC-normalized mercury levels (Hg/TOC) range between 4.5 and 85 ppb Hg/wt%TOC. Both Hg and Hg/TOC values appear elevated within the lower ~50 m of the Las Overas 1 composite section, with values up to 76 ppb Hg and 85 ppb/wt% Hg/TOC, being significantly higher compared to the underlying strata of Arroyo Serrucho F and the overlying Las Overas strata (<11 ppb Hg, 11 ppb/wt% Hg/TOC on average; Fig. 3). A similar trend is recorded in the Hg/Al and Hg/(Si/Al) (Fig. 4A), indicating that Hg enrichments are not linked to organic-matter accumulation or relative changes in the percentage of clay. Elemental sulphur measurements were largely below detection limit, suggesting drawdown and fixation of Hg by sulphide deposition did not play a significant role in the Hg accumulation in these sediments (see Sanei et al. 2012).

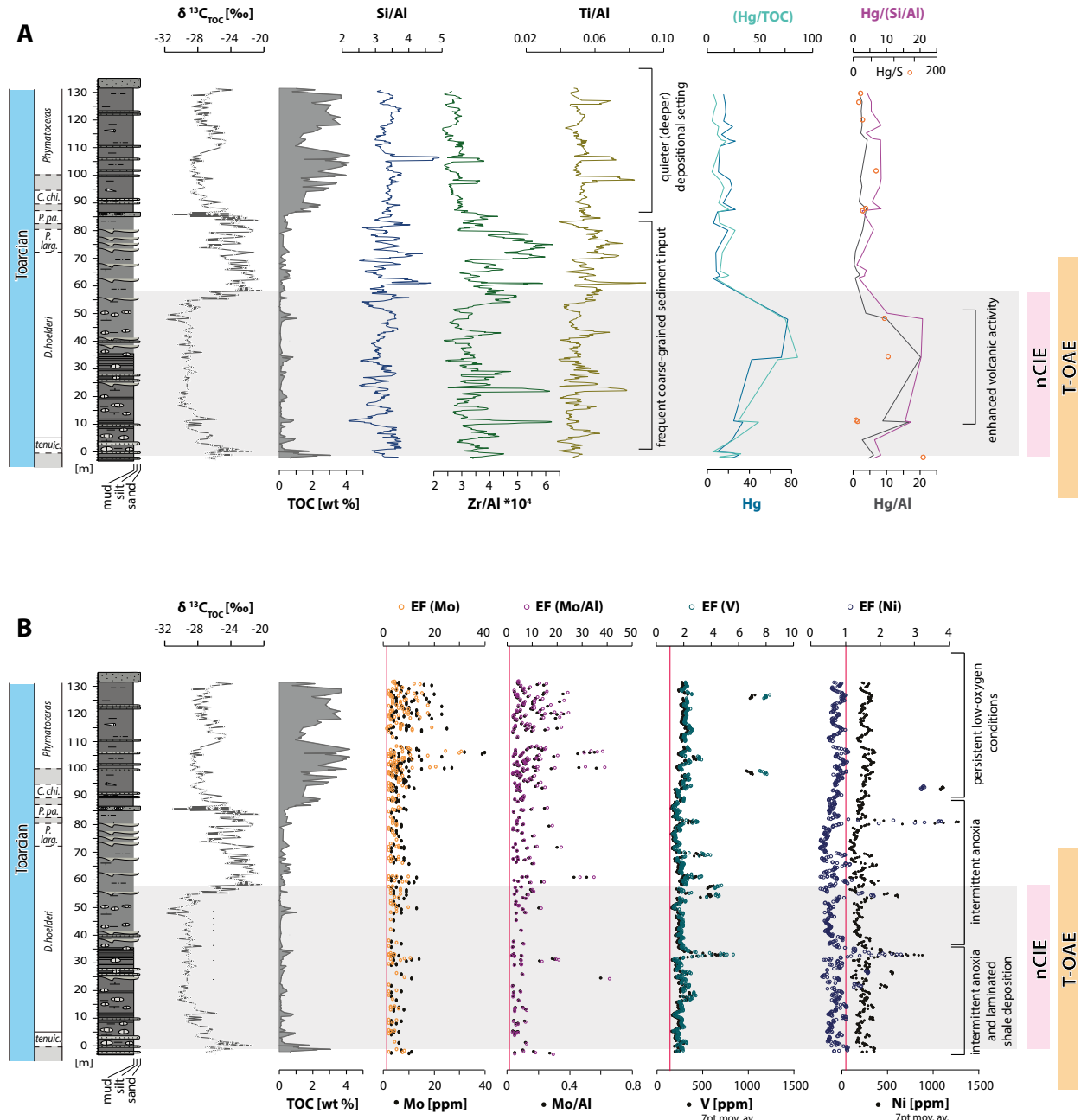


Fig. 4. Distribution of major and trace elements plotted against $\delta^{13}\text{C}_{\text{TOC}}$ and TOC. **A:** Distribution of Si, Zr, Ti (detrital elements), normalized against Al, and sedimentary Hg normalized against Al and Si/Al, S and TOC. **B:** Mo, Mo/Al, V and Ni as absolute values and enrichment factors relative to the average shale values (Wedepohl 1971). Approximate stratigraphic position of the T-OAE and nCIE intervals marked in orange, and grey/pink, respectively.

5. Discussion

5.1 Stratigraphic framework

The bivalve and brachiopod assemblages, combined with lithostratigraphic observations suggest that the Arroyo Serrucho E and F sections represent Upper

Pliensbachian strata. The ammonite *Austromorphites behrendseni* (Jaworski)? indicative for the *A. behrendseni* Zone was recovered from strata ~40 m below the base of Arroyo Serrucho E (Plate S1A). *Fanninoceras?* sp. indicative for the *F. fannini* Zone was found close to the base of Arroyo Serrucho section E

(Plate S1A). These fossil finds suggest that the strata of the two sections potentially span the *A. behrendseni* Zone to *F. disciforme* Zone.

Based on the identified ammonite assemblages, the studied strata at Las Overas represent the *tenuicostatum* Zone to lower *Dumortieria* Zone of the Lower to uppermost Toarcian according to the Andean ammonite biostratigraphic scheme (Fig. 2, Plate S1A–B). Both the top of the Las Overas 1 composite section and the base of Las Overas 2 section lie within the *Phymatoceras* Zone, demonstrating that no ammonite zones are missing in their entirety at the exposure gap. According to the correlation of the Andean ammonite zonation scheme (Fig. 2; Riccardi 2008), the stratigraphic interval studied here in the Las Overas sections is approximately equivalent to the Lower Toarcian upper *tenuicostatum* Zone to Upper Toarcian *aalensis* Zone of the NW European ammonite zonation scheme: i.e., almost the full span of the Toarcian Stage.

The studied Las Overas sections partly overlap stratigraphically with sections in the Arroyo Serrucho creek that were previously studied by Mazzini et al. (2010) and Al-Suwaidi et al. (2016) (Arroyo Serrucho sections A, B; C and D; Fig. 2 and 5). Based on the chemostratigraphic correlation of the $\delta^{13}\text{C}_{\text{TOC}}$ records, and by tracing outcrop features in the field, Arroyo Serrucho sections A and B are considered as stratigraphically equivalent to the Las Overas 1 composite section strata between ~26–60 m and ~45–53.5 m, respectively (Fig. 2 and 5). This interval is characterized by relatively low $\delta^{13}\text{C}_{\text{TOC}}$ values, followed by a sharp positive shift in $\delta^{13}\text{C}_{\text{TOC}}$ in both records.

The *tenuicostatum*–*D. hoelderi* boundary at Las Overas is placed at 5 m based on the LwO of *Dactyloceras* (*Orthodactylites*) cf. *hoelderi* (Hillebrandt & Schmidt-Effing). This stratigraphic position is 38 m lower in the succession relative to where it was previously identified in the Arroyo Serrucho section based on the LwO of *Harpoceras* cf. *serpentinum* (Schlotheim) (Fig. 5; Al-Suwaidi et al. 2016). The stratigraphic position of the *tenuicostatum*–*D. hoelderi* zonal boundary proposed herein is based on fossil finds of hitherto unstudied strata and is also supported by the chemostratigraphic correlation of the $\delta^{13}\text{C}_{\text{TOC}}$ record (see section 5.2).

The correlation between the Las Overas 1 composite section and Arroyo Serrucho C and D is based on lithostratigraphy (Fig. 5). The condensed, phosphate- and fossil-rich stratigraphic marker bed occurring between 85.4–86.4 m in the Las Overas 1 composite section, likely marking an interval of condensation and

hiatus, has also been identified in the Arroyo Serrucho section C and D (~5.60–6.40 m) (Mazzini et al. 2010, Al-Suwaidi et al. 2016). Anchored to this marker bed (assuming that it is time-equivalent in the two sections), there is excellent correlation between the $\delta^{13}\text{C}_{\text{TOC}}$ trends documented at Arroyo Serrucho C and D and the Las Overas 1 composite section between ~78–134 m (Fig. 5).

Based on this correlation, in both sections the *P. pacificum* Zone and *C. chilensis* Zone have a comparable stratigraphic thickness (Fig. 5). Both ammonite zones appear condensed relative to the underlying and overlying strata. Constraints on the age of the phosphate-rich marker bed recorded here to the *P. pacificum* Zone appears relevant for a better understanding of the so-called “intra-Toarcian discontinuity/unconformity” recognized in subsurface studies elsewhere in the Neuquén Basin (e.g., Pángaro et al. 2006).

5.2 Stratigraphic correlation of the Andean *tenuicostatum*–*D. hoelderi* and European *tenuicostatum*–*serpentinum* zonal boundaries

Due to the proximity of the Neuquén Basin to the Andean volcanic arc during the Early Jurassic (Fig. 1B), the strata in the basin are intercalated with volcanic ash beds. These ash beds allow age determination of the strata with absolute dating methods. In European sections, such an approach is not possible due to the lack of intercalated volcanic material. Combined chemo- and biostratigraphic control on both Andean and coeval NW European sections enables a precise correlation of data from both hemispheres, including conflation of absolute and relative age constraints that allows generation of a robust geological time scale.

The *tenuicostatum*–*D. hoelderi* zonal boundary at the Las Overas 1 composite section is positioned at the stepwise transition to lower $\delta^{13}\text{C}_{\text{TOC}}$ values at the onset of the nCIE, more precisely at the rising limb of a positive shift in $\delta^{13}\text{C}_{\text{TOC}}$ within the superimposed negative trend (Fig. 6A–B). The NW European equivalent to the *tenuicostatum*–*D. hoelderi* zonal boundary is the *tenuicostatum*–*serpentinum* zonal boundary. Correlation of the $\delta^{13}\text{C}_{\text{TOC}}$ record of the Las Overas 1 composite section to the schematic composite $\delta^{13}\text{C}$ curve, which is based on the compilation of numerous high-resolution carbon-isotope records (see Ruebsam & Al-Husseini 2020 for overview, Fig. 6A, B) and the biostratigraphically well-calibrated high-resolution $\delta^{13}\text{C}$ record of the Mochras core (Xu et al. 2018b),

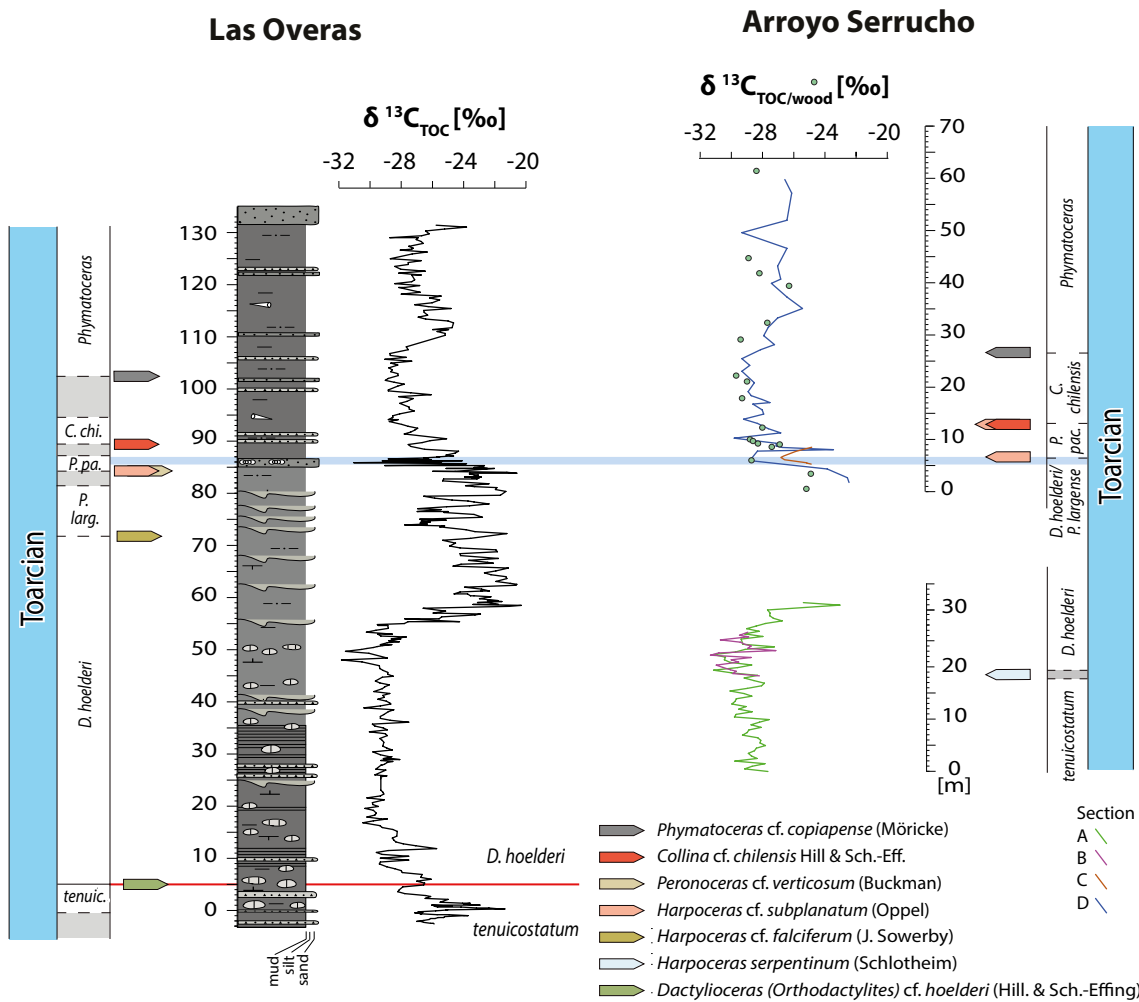
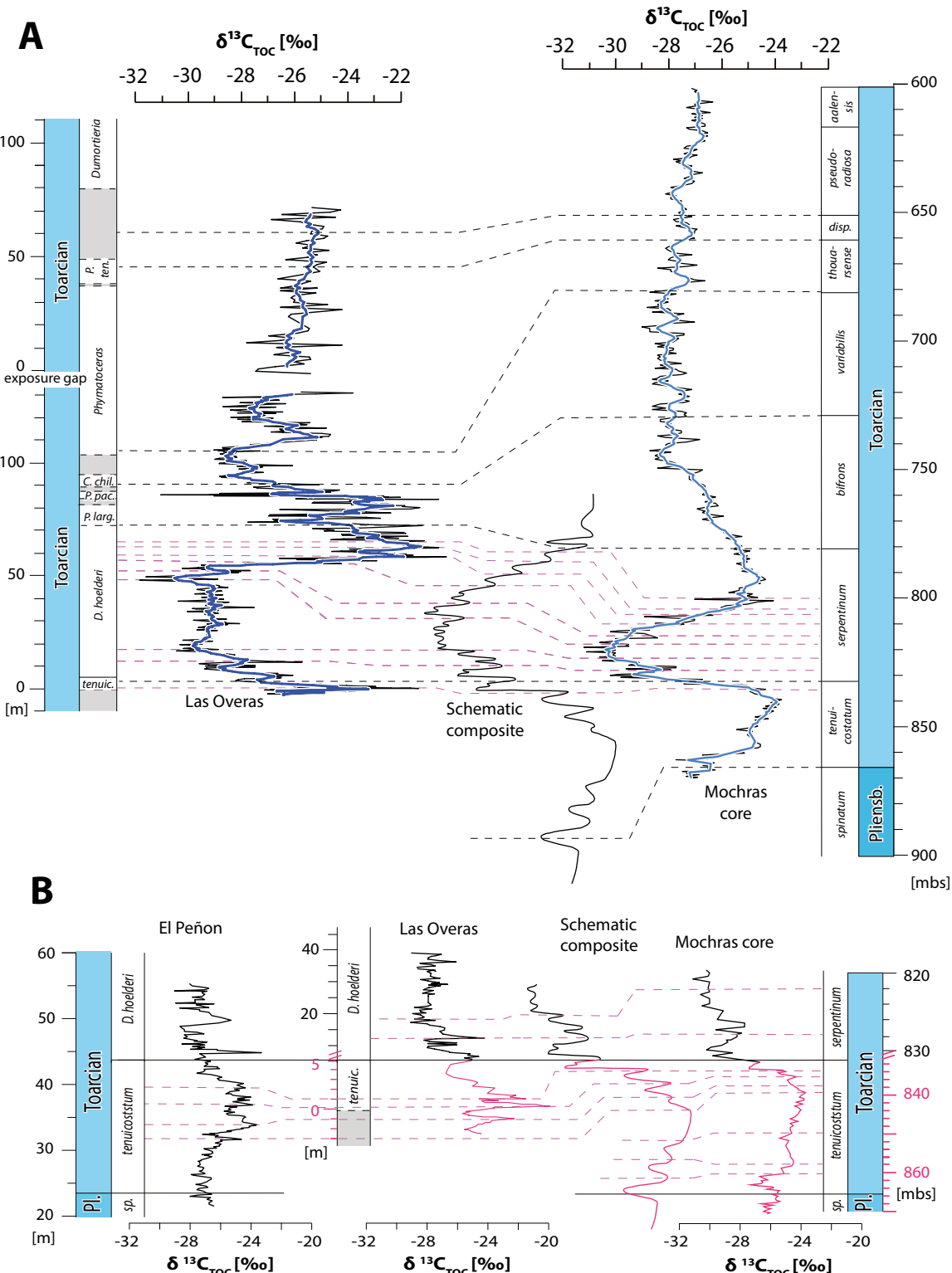


Fig. 5. Bio- and chemostratigraphic correlation of the Las Overas 1 composite section and Arroyo Serrucho sections. Serrucho data from Mazzini et al. (2010) and Al-Suwaidi et al. (2016). The new stratigraphic position of the *tenuicostatum*-*D. hoelderi* zonal boundary proposed herein is shown by a red line. Note that the correlation between Las Overas 1 composite section and Arroyo Serrucho section A and B is based on chemostratigraphic data. The correlation to Arroyo Serrucho section C and D is based on the lithostratigraphic correlation of the condensed stratigraphic marker bed indicated by the light blue line. The stratigraphic position of the key fossils for the biostratigraphic interpretation are shown in the figure. Stratigraphic logs including all recovered invertebrate fossils can be found in supplementary figures S1, S3 and S4.

Fig. 6. Correlation of the Las Overas $\delta^{13}\text{C}_{\text{TOC}}$ record with other sections **A:** Correlation of the Las Overas $\delta^{13}\text{C}_{\text{TOC}}$ record with the Mochras (Llanbedr, Wales, UK) drill-core, Cardigan Bay Basin (Xu et al. 2018b, Storm et al. 2020) with revised ammonite zonation after McArthur et al. (2016), and the idealized schematic $\delta^{13}\text{C}$ record of the T-OAE based on the multiple biostratigraphically calibrated high-resolution carbon-isotope records after Ruebsam & Al-Husseini (2020). Black dashed lines indicate correlation of biozones after Riccardi (2008). Purple dashed lines correlate individual shifts in $\delta^{13}\text{C}$. **B:** Correlation of the $\delta^{13}\text{C}$ record of the *tenuicostatum* and *D. hoelderi/serpentinum* zones of Las Overas, El Peñon, (Chile, Fantasia et al. 2018), Mochras and the schematic $\delta^{13}\text{C}$ curve (see above). Dashed lines represent correlation tie-points after Ruebsam & Al-Husseini (2020) that were expanded to fit the Las Overas composite and El Peñon sections. Note the different scales of Las Overas and Mochras in the correlation of the *tenuicostatum* Zone and *D. hoelderi/serpentinum* Zone. Geographic location of individual sections shown in Fig. 1A-B.



show that the *tenuicostatum–serpentinum* zonal boundary corresponds to the same pattern (positive shift within stepwise decrease) in the isotope record, albeit with a small stratigraphic offset, since the boundary at Mochras corresponds to the falling limb of the positive isotope shift, i.e. stratigraphically higher. However, the *tenuicostatum–D. hoelderi* zonal boundary and *tenuicostatum–serpentinum* zonal boundary both correspond to the same pattern in $\delta^{13}\text{C}_{\text{TOC}}$.

Cyclostratigraphic duration estimates of the individual shifts in $\delta^{13}\text{C}_{\text{TOC}}$ that are widely recorded throughout the Lower Toarcian suggest that the negative CIE associated with the boundary lasted ~10s–100s of kyrs (e.g., Pienkowski et al. 2024). The temporal difference associated with the stratigraphic offset of the boundary is therefore likely less than 100 kyr and the boundary can be inferred as nearly synchronous in the NW European and Andean realm.

Expanding the correlation exercise to the strata stratigraphically below the *tenuicostatum–D. hoelderi* zonal boundary (Fig. 6B, 7), the pattern recorded at Las Overas 1 suggests that a large part of the *tenuicostatum* Zone may be present in the studied interval, albeit highly condensed compared with the overlying *D. hoelderi* strata. However, bio- and chemostratigraphic data from the strata below the Las Overas 1 composite section are needed to confirm the suggested correlation.

5.3 Identification of the T-OAE interval at Las Overas

Based on the correlation of the Andean and European ammonite schemes, the nCIE recorded in the *tenuicostatum* Zone to mid-*D. hoelderi* Zone at Las Overas is stratigraphically equivalent to the nCIE recorded in the *tenuicostatum* to *serpentinum* zones in NW Europe (Fig. 2, Riccardi 2008). This nCIE is interpreted as the carbon-isotopic fingerprint that invariably records the global carbon-cycle perturbation documented in records of the T-OAE worldwide.

Correlation of the $\delta^{13}\text{C}_{\text{TOC}}$ record to the Mochras drill-core (Xu et al. 2018b) and the schematic composite $\delta^{13}\text{C}_{\text{TOC}}$ curve of Ruebsam & Al-Husseini (2020) indicates that Las Overas data record the CIE from the very onset of the negative shift. The $\delta^{13}\text{C}_{\text{TOC}}$ record at Las Overas resembles the global signal including the stepwise shift towards lower isotope values. The segment of the nCIE recording the most negative values appears stratigraphically expanded, with the interval

of most negative $\delta^{13}\text{C}_{\text{TOC}}$ values measuring ~35 m in thickness.

The observed increase in sedimentary Hg and Hg/TOC, which appears independent of changes in the lithofacies (Fig. 4A), moves in parallel with the negative $\delta^{13}\text{C}_{\text{TOC}}$ values in the *D. hoelderi* Zone. The similarity between these trends and those normalized to Al and Si/Al and TOC further suggests that the Hg enrichment was not driven by changes in the sedimentary input, nor by enhanced influx of organic material. Comparable increases in sedimentary Hg concentrations, appearing concomitantly with the nCIE associated with the T-OAE, have previously been detected in geographically widely distributed Lower Toarcian sections of upper *tenuicostatum* and *serpentinum* ammonite standard zonal age (and corresponding local equivalents), including other sections in the Neuquén Basin (e.g., Percival et al. 2015, Fantasia et al. 2018, Them et al. 2019, Al-Suwaidi et al. 2022, Ruhl et al. 2022). Thus, the record of a Hg/TOC enrichment in the lower Las Overas strata that are considered to document the T-OAE based on biostratigraphic and carbon-isotope data is consistent with previous interpretations of a pronounced mercury-cycle perturbation taking place in the Neuquén Basin at that time, likely reflecting the more global-scale disturbance reported from many other sites. The mercury-cycle perturbation associated with the T-OAE is generally considered to have been related to the increased volcanic and/or thermogenic emissions of the element to the atmosphere during emplacement of the Karoo-Ferrar LIP (Percival et al. 2015, Svensen et al. 2023, Fendley et al. 2024) as well as potentially the Chon-Aike siliciclastic LIP-style Province (Pankhurst et al. 2000). However, the lack of such peaks in a minority of T-OAE records emphasises that this Hg output likely entered the marine realm variably, potentially via terrestrial recycling and riverine runoff in some locations (Them et al. 2019). Thus, whilst the Hg and Hg/TOC peaks at Las Overas are consistent with many other T-OAE sites, they cannot be used as a stratigraphic marker of the T-OAE interval in and of themselves.

5.4 Organic-matter preservation and redox changes

Strata deposited during the T-OAE, more specifically within the nCIE interval, are widely associated with elevated TOC levels relative to the underlying and overlying sediments, as known from geographically widespread sections representing various depositional

settings (e.g., Jenkyns 1988, 2010; Jenkyns et al. 2002, Gröcke et al. 2011, Al-Suwaidi et al. 2016, Xu et al. 2017, Ikeda et al. 2018, Liu et al. 2020, Silva et al. 2021a, Filatova et al. 2022, Kemp et al. 2022, Gambacorta et al. 2024, Ruebsam & Schwark 2024). The phenomenon is conventionally linked to temperature-driven acceleration of the hydrogeological cycle, increased freshwater and nutrient input into the oceans, and subsequent productivity- and stratification-driven anoxia leading to organic-matter preservation (Jenkyns 2010). Within the European realm, organic-rich sediments are widely distributed in the restricted northern epicontinental European seaway. Conversely, strata deposited in some more southerly Tethyan localities (e.g., High Atlas, Morocco; Lusitanian Basin, Portugal; Betic Cordillera, Spain; Southern Alps of Italy) as well as northern Chile (southwestern Gondwana) are comparatively organic-lean and generally lack geochemical evidence for bottom-water anoxia (e.g., van de Schootbrugge et al. 2005, Bodin et al. 2010, Suan et al. 2013, Krencker et al. 2015, Fantasia et al. 2018, 2019, Ruvalcaba Baroni et al. 2018, Silva et al. 2021b, Erba et al. 2022, Gambacorta et al. 2024, Ruebsam & Schwark 2024). These spatial differences in organic-matter preservation have been attributed to diverse palaeogeographic settings, regional circulation patterns, climate-driven nutrient supply and primary productivity, and intensified storm activity and basin-ward shift of the storm weather wave base during the T-OAE.

Previously studied sections located in the central and southern part of the Neuquén Basin exhibit increased organic-matter preservation associated with the T-OAE interval. The Chacay Melehue section (central Neuquén Basin) is associated with TOC levels of up to 4.2 wt% in the mid-*tenuicostatum* Zone (Al-Suwaidi et al. 2022). At Arroyo Lapa South (southern Neuquén Basin), TOC values of up to 11 wt% are reported from the stratigraphic interval associated with the T-OAE nCIE (Al-Suwaidi et al. 2016). An exception is Arroyo Lapa North, located adjacent to Arroyo Lapa South, where TOC levels appear to have not increased. This apparent spatial variance is likely due to local sediment erosion and re-deposition in a deep-sea fan complex.

The T-OAE strata deposited in the northern Neuquén Basin at Las Overas and Arroyo Serrucho manifest strikingly low TOC values (<1 wt% on average; Fig. 7), even considering the thermally over-mature setting (Al-Suwaidi et al. 2016, and this study), and evidence for persistent oxygen-depletion is lacking.

However, individual stratigraphic intervals record a rise in TOC to 1–3 wt% with a concomitant increase in redox-sensitive trace elements (Fig. 4B). This geochemical pattern suggests that intermittent oxygen depletion did occur within this palaeoenvironment. Evidence for these brief shifts towards low-oxygen conditions were not restricted to the stratigraphic interval associated with the T-OAE nCIE, but also appear stratigraphically above the nCIE and T-OAE interval up to the *P. pacificum* Zone (Fig. 6B) suggesting that reducing conditions did intermittently develop long after the cessation of the anoxic event itself. This decoupling of organic carbon burial from the nCIE has been observed in few other sections from different palaeogeographic settings and linked to local depositional conditions (Ruebsam & Schwark 2024).

At Las Overas, more persistent low-oxygen conditions developed concomitantly with the deepening of the depositional environment indicated by the change in lithology towards more fine-grained mudstone (Fig. 4A, B, S1). However, only within the stratigraphic intervals associated with the lower part of the nCIE (up to ~35 m), are the brief intervals of TOC- and trace-metal enrichment associated with laminated facies. The preservation of these laminae is characteristic of organic-rich T-OAE deposits and reflects a lack of benthonic fauna linked to the low-oxygen environment, pointing towards the intermittent development of more severe anoxia relative to conditions under which younger strata were deposited.

It is likely that multiple environmental factors inhibited the development of persistent oxygen depletion and black-shale deposition within the nCIE interval at Las Overas in contrast to the coeval organic-rich deposits in the central and southern Neuquén Basin. These processes possibly comprised a combination of basin development (subsidence), net sedimentation rate, current dynamics (e.g., Las Overas was situated close to the Curepto Strait, connecting the basin to the open ocean), and climate: processes similar to those postulated for the T-OAE interval in the southern Tethyan realm. The low-TOC strata at Las Overas are characterized by the common occurrence of hummocky cross-laminated sandstones comprising fossil debris and possessing erosive basal surfaces, here interpreted to represent storm deposits. The frequent supply of storm deposits suggests a depositional setting in which the organic-matter preservation was diminished by the recurring supply of oxygen into the deeper basin. Sedimentological evidence from the western Tethyan area (Suan et al. 2013, Krencker et al. 2015, Fantasia et al.

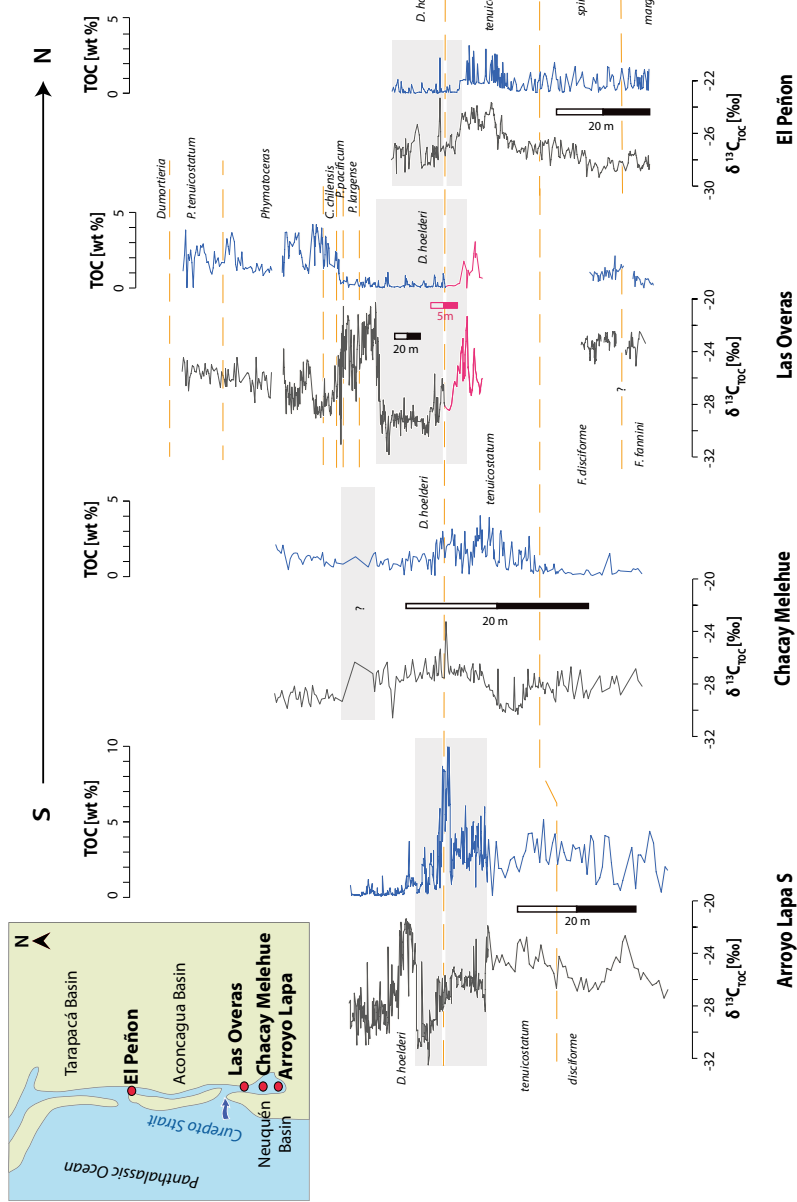


Fig. 7. Correlation of $\delta^{13}\text{C}_{\text{TOC}}$ and TOC profiles recorded from the Andean Basin along the western margin of Gondwana in Chile (El Peñón; Fantasia et al. 2018), the northern Neuquén Basin (Las Obras; this study), the central Neuquén Basin (Chacay Melehue; Al-Suwaidi et al. 2022) and southern Neuquén Basin (Arroyo Lapa South; Al-Suwaidi et al. 2010). Note that Arroyo Lapa North was excluded from the correlation exercise because the stratigraphic record is likely disturbed by local sediment redeposition. Light grey bar indicates the approximate nCIE interval associated with the T-OAE. Geographic location of individual sections shown in figure.

2019) and the eastern Tethyan margin (Han et al. 2018) suggest intensification of tropical cyclones and storms, associated with a deepening of the mean storm weather wave base related to the greenhouse conditions prevailing during the T-OAE. In the Chilean Andean Basin, representative for the south-western Gondwana margin, the onset of the T-OAE was also coupled with an increase in storm events (Fantasia et al. 2018). In this Chilean basin, clay mineralogy suggests a simultaneous shift towards more arid conditions, likely resulting in a decrease in nutrient input, thereby limiting productivity-driven development of anoxia and organic-matter preservation (Fantasia et al. 2018).

At Las Overas, the common occurrence of storm deposits may, however, not be linked to climatic change associated with the T-OAE. Rather, these levels may reflect the depositional setting and relative sea-level changes: the T-OAE and associated palaeoenvironmental disturbance terminated within the *serpentinium* Zone (e.g., Erba et al. 2022), of which the *D. hoelderi* Zone represents the local equivalent in the Andean realm. The occurrence of storm deposits at Las Overas, however, reaches into the upper *P. largaense* Zone. A shift to more permanent oxygen-depleted conditions at the time is indicated by the concomitant increase in Mo/Al, V, Ni and TOC from the stratigraphic marker bed (at 85.4 m) in the *P. largaense* Zone and stratigraphically upwards. In this part of the section, the coeval transition towards finer grained strata suggests a general deepening of the depositional environment associated with lower oxygen conditions.

Differential syn-sedimentary subsidence within different parts of the Neuquén Basin may also have led to higher sedimentation rates in the northern part, resulting in a higher rate of sediment dilution in this area. A high sedimentation rate is evident when the stratigraphic thickness of the T-OAE interval is compared to coeval sections: the segment recording the most negative carbon-isotope values of the T-OAE nCIE in Las Overas is ~55 m thick, which is approximately 2.5 times the stratigraphic thickness of coeval strata in the Mochras drill-core from the Cardigan Bay Basin (UK) (~22 m; Fig. 6A), which is regarded as one of the most expanded Lower Toarcian successions of the north-west European realm (Xu et al. 2018b). Conversely, the same segment of the isotope curve recorded in the organic-rich Arroyo Lapa section (Fig. 7) covers ~7 m, implying a considerably lower sedimentation rate and thus less dilution of sedimentary organic matter by clastic material on the seafloor (as proposed for other sites by Kemp et al. 2022).

However, sediment dilution might have played only a secondary role in diminishing the organic-matter enrichment during the T-OAE, as there is no clear correlation between basin subsidence/sedimentation rate, and TOC in the strata stratigraphically above the T-OAE interval. This phenomenon is manifested in the *P. largaense* Zone and *P. pacificum* Zone, for example, which appear stratigraphically condensed relative to the underlying *D. hoelderi* Zone, although TOC remains low (see Fig. 3). However, the *Phymatoceras* Zone, which appears stratigraphically expanded, suggesting relatively high sedimentation rates, is characterized by moderate TOC values of 1 to 4 wt%. The increase in organic-matter preservation seems to be linked to a general deepening of the accumulation environment caused by the interplay of subsidence rates/sea-level rise and sediment supply, as evidenced by the lithological change to finer grained strata lacking storm deposits concomitantly with the increase in TOC.

The proximity of Las Overas to the Curepto Strait (Fig. 1B, 7) might have been associated with the influx of oxygen-rich ocean water, which may have supplied the basin with nutrients, but simultaneously led to persistently agitated/dynamic oxygenated conditions and strong currents in the relatively narrow northern part of the Neuquén Basin (at Las Overas and Arroyo Serrucho). The organic-rich strata of Arroyo Lapa and Chacay Melehue were located in the much wider central and southern Neuquén Basin, relatively distant from the Curepto Strait, and likely experienced quieter conditions that possibly led to sustained low-oxygen levels favourable for the preservation of organic matter.

6. Conclusions

The new biostratigraphically calibrated geochemical data from the Las Overas sections located in the northern part of the Neuquén Basin of Argentina provide a stratigraphically extended high-resolution record of Upper Pliensbachian strata and the sediments of the Lower Toarcian uppermost *tenuicostatum* Zone to the Upper Toarcian *Dumortieria* Zone, equivalent to the *tenuicostatum* to upper *pseudoradiosa* European ammonite zones. This study presents the first geochemical record from the Southern Hemisphere covering almost the entire Toarcian and thereby both the T-OAE and post-T-OAE strata. Based on fossil finds, the zonal boundary between the *tenuicostatum* Zone and *D. hoelderi* Zone is re-defined in the Las Overas 1 composite

section presented here. Correlation of the geochemical data from the *tenuicostatum*–*D. hoelderi* zonal boundary of the Andean realm and the *tenuicostatum*–*serpentinum* zonal boundary of the NW European realm supports near-synchronicity of the ammonite zonal boundaries. Differences in organic-matter preservation throughout the *D. hoelderi* Zone and *P. pacificum* Zone within the Neuquén Basin may be linked to the interplay of relative sea-level changes and local sedimentation rates as a function of syn-sedimentary tectonics and ocean dynamics: factors controlling the development of anoxia and sediment dilution on a local to regional scale. These factors likely also inhibited the development of persistent anoxia during the carbon-cycle perturbation associated with the T-OAE at Las Overas, in contrast to the coeval deposition of organic-rich facies in the central and southern parts of the Neuquén Basin.

Acknowledgements. We thank Steve Wyatt (Oxford University) for laboratory assistance, and the Stable Isotope Analytical Facilities of the Open University, Milton Keynes. We acknowledge funding from Shell International Exploration & Production B.V. M.S.S. acknowledges funding from the Netherlands Earth Science Centre (NESSC). L.M.E. Percival acknowledges funding from the Natural Environment Research Council Grant NE/G01700X/1, PhD studentship NE/L501530/1, and Research Foundation–Flanders (FWO) grant 12P4522N. S.P. Hesselbo acknowledges funding from the UK Natural Environment Research Council (NE/N018508/1). This paper is a contribution to the Early Jurassic Timescale and Earth System research project (JET). S.E.D., M.O.M. and A.C.R. were financially supported by CONICET (National Research Council of Argentina). We thank S. Wohlwend, the anonymous reviewer, and Editor J. Erbacher for constructive feedback that significantly improved this manuscript. For the purpose of open access, the author has applied a ‘Creative Commons Attribution (CC BY) licence to any Author Accepted Manuscript version arising from this submission.

Author contributions

All authors were involved in either field work, sample analysis and preparation and data interpretation. Additionally, all authors were involved in editing the manuscript and provided comments on the text, figures and supplementary data. Specific details are as follows: M.S.S. – field sampling, sample preparation and analysis (carbon isotopes, Rock-Eval analysis, HH-XRF), data interpretation, authoring and illustrating the paper. S.P.H. – field work, data interpretation, discussion and editing. H.C.J. – field work, data interpretation, discussion and editing. M.R. – field work, data interpretation, discussion and editing. A.H.A. – field

work, data interpretation, illustrating Suppl. Fig 2, discussion and editing. L.M.E.P. and T.A.M. – analysis of Hg, data interpretation, discussion and editing. S.E.D.; M.O.M. & A.C.R. – field work and logistical support, bivalve, brachiopod and ammonite biostratigraphy, data interpretation, discussion and editing.

Competing interests

The authors declare no competing interests.

References

- Al-Suwaidi, A. H., Angelozzi, G. N., Baudin, F., Damborenea, S. E., Hesselbo, S. P., Jenkyns, H. C., . . . Riccardi, A. C. (2010). First record of the Early Toarcian oceanic anoxic event from the Southern Hemisphere, Neuquén Basin, Argentina. *Journal of the Geological Society*, 167(4), 633–636. <https://doi.org/10.1144/0016-76492010-025>
- Al-Suwaidi, A. H., Hesselbo, S. P., Damborenea, S. E., Manceñido, M. O., Jenkyns, H. C., Riccardi, A. C., . . . Baudin, F. (2016). The Toarcian Oceanic Anoxic Event (Early Jurassic) in the Neuquén Basin, Argentina: A reassessment of age and carbon isotope stratigraphy. *The Journal of Geology*, 124(2), 171–193. <https://doi.org/10.1086/684831>
- Al-Suwaidi, A. H., Ruhl, M., Jenkyns, H. C., Damborenea, S. E., Mancenido, M. O., Condon, D. J., . . . Hesselbo, S. P. (2022). New age constraints on the Lower Jurassic Pliensbachian–Toarcian Boundary at Chacay Melehue (Neuquén Basin, Argentina). *Scientific Reports*, 12(1), 4975. <https://doi.org/10.1038/s41598-022-07886-x>
- Bailey, T., Rosenthal, Y., McArthur, J., Van De Schootbrugge, B., & Thirlwall, M. (2003). Paleoceanographic changes of the Late Pliensbachian–Early Toarcian interval: A possible link to the genesis of an Oceanic Anoxic Event. *Earth and Planetary Science Letters*, 212(3–4), 307–320. [https://doi.org/10.1016/S0012-821X\(03\)00278-4](https://doi.org/10.1016/S0012-821X(03)00278-4)
- Behar, F., Beaumont, V., & Penteado, H. D. B. (2001). Rock-Eval 6 technology: Performances and developments. *Oil & Gas Science and Technology*, 56, 111–134. <https://doi.org/10.2516/ogst:2001013>
- Bin, C., Xiaoru, W., & Lee, F. S. (2001). Pyrolysis coupled with atomic absorption spectrometry for the determination of mercury in Chinese medicinal materials. *Analytica Chimica Acta*, 447(1–2), 161–169. [https://doi.org/10.1016/S0003-2670\(01\)01218-1](https://doi.org/10.1016/S0003-2670(01)01218-1)
- Blakey, R. (2007). Early Jurassic rectangular paleogeographic map in Mollweide. <http://jan.ucc.nau.edu/rbc7/200marect.jpg>
- Bodin, S., Mattioli, E., Fröhlich, S., Marshall, J. D., Boutib, L., Lahsini, S., & Redfern, J. (2010). Toarcian carbon isotope shifts and nutrient changes from the Northern margin of Gondwana (High Atlas, Morocco, Jurassic): Palaeoenvironmental implications. *Palaeogeography, Palaeoclimatology, Palaeoecology*, 297(2), 377–390. <https://doi.org/10.1016/j.palaeo.2010.08.018>

- Burgess, S. D., Bowring, S. A., Fleming, T. H., & Elliot, D. H. (2015). High-precision geochronology links the Ferrar large igneous province with early-Jurassic ocean anoxia and biotic crisis. *Earth and Planetary Science Letters*, 415, 90–99. <https://doi.org/10.1016/j.epsl.2015.01.037>
- Calvert, S., & Pedersen, T. (2007). Chapter fourteen elemental proxies for palaeoclimatic and palaeoceanographic variability in marine sediments: Interpretation and application. *Developments in Marine Geology*, 1, 567–644. [https://doi.org/10.1016/S1572-5480\(07\)01019-6](https://doi.org/10.1016/S1572-5480(07)01019-6)
- Dahl, T. W., Ruhl, M., Hammarlund, E. U., Canfield, D. E., Rosing, M. T., & Bjerrum, C. J. (2013). Tracing euxinia by molybdenum concentrations in sediments using hand-held X-ray fluorescence spectroscopy (HHXRF). *Chemical Geology*, 360–361, 241–251. <https://doi.org/10.1016/j.chemgeo.2013.10.022>
- Damborenea, S. E. (1987). Early Jurassic Bivalvia of Argentina. Part 1: Stratigraphical introduction and superfamilies Nuculanacea, Arcacea, Mytilacea and Pinnacea. *Palaeontographica. Abteilung A, Paläozoologie, Stratigraphie*, 199, 23–111.
- Damborenea, S. E. (2002). Early Jurassic bivalves of Argentina. Part 3: Superfamilies Monotoidea, Pectinoidea, Placatuloidea and Dimyoidea. *Palaeontographica. Abteilung A, Paläozoologie, Stratigraphie*, 265(1–4), 1–119. <https://doi.org/10.1127/pala/265/2002/1>
- Dera, G., Brigaud, B., Monna, F., Laffont, R., Pucéat, E., Deconinck, J.-F., . . . Durlet, C. (2011). Climatic ups and downs in a disturbed Jurassic world. *Geology*, 39(3), 215–218. <https://doi.org/10.1130/G31579.1>
- Dickson, A. J., Gill, B. C., Ruhl, M., Jenkyns, H. C., Porcelli, D., Idiz, E., . . . van den Boorn, S. H. J. M. (2017). Molybdenum-isotope chemostratigraphy and paleoceanography of the Toarcian Oceanic Anoxic Event (Early Jurassic). *Paleoceanography*, 32(8), 813–829. <https://doi.org/10.1002/2016PA003048>
- Echevarría, J., Damborenea, S. E., & Manceñido, M. O. (2021). Early Jurassic Trigoniida (Bivalvia) from Argentina. *Journal of Paleontology*, 95(S85), 1–55. <https://doi.org/10.1017/jpa.2021.43>
- Erba, E., Cavalheiro, L., Dickson, A. J., Faucher, G., Gambacorta, G., Jenkyns, H. C., & Wagner, T. (2022). Carbon- and oxygen-isotope signature of the Toarcian Oceanic Anoxic Event: Insights from two Tethyan pelagic sequences (Gajum and Sogno Cores – Lombardy Basin, northern Italy). *Newsletters on Stratigraphy*, 55(4), 451–477. <https://doi.org/10.1127/nos/2022/0690>
- Fantasia, A., Föllmi, K. B., Adatte, T., Bernárdez, E., Spangenberg, J. E., & Mattioli, E. (2018). The Toarcian oceanic anoxic event in southwestern Gondwana: An example from the Andean basin, northern Chile. *Journal of the Geological Society*, 175(6), 883–902. <https://doi.org/10.1144/jgs2018-008>
- Fantasia, A., Adatte, T., Spangenberg, J. E., Font, E., Duarte, L. V., & Föllmi, K. B. (2019). Global versus local processes during the Pliensbachian–Toarcian transition at the Peniche GSSP, Portugal: A multi-proxy record. *Earth-Science Reviews*, 198, 102932. <https://doi.org/10.1016/j.earscirev.2019.102932>
- Fendley, I. M., Frieling, J., Mather, T. A., Ruhl, M., Hesselbo, S. P., & Jenkyns, H. C. (2024). Early Jurassic large igneous province carbon emissions constrained by sedimentary mercury. *Nature Geoscience*, 17(3), 241–248. <https://doi.org/10.1038/s41561-024-01378-5>
- Filatova, N. I., Konstantinovskaya, E., & Vishnevskaya, V. (2022). Jurassic-Lower Cretaceous siliceous rocks and black shales from allochthonous complexes of the Koryak-Western Kamchatka orogenic belt, East Asia. *International Geology Review*, 64(3), 311–330. <https://doi.org/10.1080/00206814.2020.1848649>
- Franzese, J. R., & Spalletti, L. A. (2001). Late Triassic–early Jurassic continental extension in southwestern Gondwana: Tectonic segmentation and pre-break-up rifting. *Journal of South American Earth Sciences*, 14(3), 257–270. [https://doi.org/10.1016/S0895-9811\(01\)00029-3](https://doi.org/10.1016/S0895-9811(01)00029-3)
- Franzese, J. R., Spalletti, L. A., Gómez-Pérez, I., & Macdonald, D. (2003). Tectonic and paleoenvironmental evolution of Mesozoic sedimentary basins along the Andean foothills of Argentina (32°–54°S). *Journal of South American Earth Sciences*, 16(1), 81–90. [https://doi.org/10.1016/S0895-9811\(03\)00020-8](https://doi.org/10.1016/S0895-9811(03)00020-8)
- Franzese, J. R., Veiga, G. D., Schwarz, E., & Gómez-Pérez, I. (2006). Tectonostratigraphic evolution of a Mesozoic graben border system: The Chachil depocentre, southern Neuquén Basin, Argentina. *Journal of the Geological Society*, 163(4), 707–721. <https://doi.org/10.1144/0016-764920-082>
- Gambacorta, G., Brumsack, H. J., Jenkyns, H. C., & Erba, E. (2024). The early Toarcian Oceanic Anoxic Event (Jenkyns Event) in the Alpine-Mediterranean Tethys, north African margin, and north European epicontinental seaway. *Earth-Science Reviews*, 248, 104636. <https://doi.org/10.1016/j.earscirev.2023.104636>
- Grasby, S. E., Beauchamp, B., Bond, D. P. G., Wignall, P. B., & Sanei, H. (2016). Mercury anomalies associated with three extinction events (Capitanian Crisis, Latest Permian Extinction and the Smithian/Spathian Extinction) in NW Pangea. *Geological Magazine*, 153(2), 285–297. <https://doi.org/10.1017/S0016756815000436>
- Grasby, S. E., Them, T. R., II, Chen, Z., Yin, R., & Ardakani, O. H. (2019). Mercury as a proxy for volcanic emissions in the geologic record. *Earth-Science Reviews*, 196, 102880. <https://doi.org/10.1016/j.earscirev.2019.102880>
- Gröcke, D., Hori, R., Trabucho-Alexandre, J., Kemp, D., & Schwark, L. (2011). An open ocean record of the Toarcian oceanic anoxic event. *Solid Earth*, 2(2), 245–257. <https://doi.org/10.5194/se-2-245-2011>
- Gulisano, C. A., & Gutiérrez Pleimling, A. R. (1995). *Field Guide: The Jurassic of the Neuquén Basin. b) Mendoza Province*. Buenos Aires: Asociación Geológica Argentina.
- Han, Z., Hu, X., Kemp, D. B., & Li, J. (2018). Carbonate-platform response to the Toarcian Oceanic Anoxic Event in the southern hemisphere: Implications for climatic change and biotic platform demise. *Earth and*

- Planetary Science Letters*, 489, 59–71. <https://doi.org/10.1016/j.epsl.2018.02.017>
- Heimdal, T. H., Goddérus, Y., Jones, M. T., & Svensen, H. H. (2021). Assessing the importance of thermogenic degassing from the Karoo Large Igneous Province (LIP) in driving Toarcian carbon cycle perturbations. *Nature Communications*, 12(1), 6221. <https://doi.org/10.1038/s41467-021-26467-6>
- Hesselbo, S. P., Gröcke, D. R., Jenkyns, H. C., Bjerrum, C. J., Farrimond, P., Morgans Bell, H. S., & Green, O. R. (2000). Massive dissociation of gas hydrate during a Jurassic oceanic anoxic event. *Nature*, 406(6794), 392–395. <https://doi.org/10.1038/35019044>
- Hesselbo, S. P., Jenkyns, H. C., Duarte, L. V., & Oliveira, L. C. (2007). Carbon-isotope record of the Early Jurassic (Toarcian) Oceanic Anoxic Event from fossil wood and marine carbonate (Lusitanian Basin, Portugal). *Earth and Planetary Science Letters*, 253(3–4), 455–470. <https://doi.org/10.1016/j.epsl.2006.11.009>
- Howell, J. A., Schwarz, E., Spalletti, L. A., & Veiga, G. D. (2005). The Neuquén Basin: an overview. In G. D. Veiga, L. A. Spalletti, J. A. Howell, & E. Schwarz (Eds.), *The Neuquén Basin, Argentina: A case study in sequence stratigraphy and basin dynamics* (pp. 1–14). London: Geological Society.
- Iglesia-Llanos, M. P., Riccardi, A. C., & Singer, S. E. (2006). Palaeomagnetic study of Lower Jurassic marine strata from the Neuquén Basin, Argentina: A new Jurassic apparent polar wander path for South America. *Earth and Planetary Science Letters*, 252(3–4), 379–397. <https://doi.org/10.1016/j.epsl.2006.10.006>
- Ikeda, M., Hori, R. S., Ikebara, M., Miyashita, R., Chino, M., & Yamada, K. (2018). Carbon cycle dynamics linked with Karoo-Ferrar volcanism and astronomical cycles during Pliensbachian-Toarcian (Early Jurassic). *Global and Planetary Change*, 170, 163–171. <https://doi.org/10.1016/j.gloplacha.2018.08.012>
- Jenkyns, H. C. (1988). The early Toarcian (Jurassic) anoxic event: stratigraphic, sedimentary and geochemical evidence. *American Journal of Science*, 288(2), 101–151. <https://doi.org/10.2475/ajs.288.2.101>
- Jenkyns, H. C. (2003). Evidence for rapid climate change in the Mesozoic–Palaeogene greenhouse world. *Philosophical Transactions of the Royal Society A. Mathematical, Physical, and Engineering Sciences*, 361(1810), 1885–1916. <https://doi.org/10.1098/rsta.2003.1240>
- Jenkyns, H. C. (2010). Geochemistry of oceanic anoxic events. *Geochemistry, Geophysics, Geosystems*, 11(3), Q03004. <https://doi.org/10.1029/2009GC002788>
- Jenkyns, H. C., & Clayton, C. J. (1986). Black shales and carbon isotopes in pelagic sediments from the Tethyan Lower Jurassic. *Sedimentology*, 33(1), 87–106. <https://doi.org/10.1111/j.1365-3091.1986.tb00746.x>
- Jenkyns, H. C., & Clayton, C. J. (1997). Lower Jurassic epicontinental carbonates and mudstones from England and Wales: Chemostratigraphic signals and the early Toarcian anoxic event. *Sedimentology*, 44(4), 687–706. <https://doi.org/10.1046/j.1365-3091.1997.d01-43.x>
- Jenkyns, H. C., Jones, C. E., Gröcke, D. R., Hesselbo, S. P., & Parkinson, D. N. (2002). Chemostratigraphy of the Jurassic System: Applications, limitations and implications for palaeoceanography. *Journal of the Geological Society*, 159(4), 351–378. <https://doi.org/10.1144/0016-764901-130>
- Kemp, D. B., Coe, A. L., Cohen, A. S., & Schwark, L. (2005). Astronomical pacing of methane release in the Early Jurassic period. *Nature*, 437(7057), 396–399. <https://doi.org/10.1038/nature04037>
- Kemp, D. B., Selby, D., & Izumi, K. (2020). Direct coupling between carbon release and weathering during the Toarcian oceanic anoxic event. *Geology*, 48(10), 976–980. <https://doi.org/10.1130/G47509.1>
- Kemp, D. B., Suan, G., Fantasia, A., Jin, S., & Chen, W. (2022). Global organic carbon burial during the Toarcian oceanic anoxic event: Patterns and controls. *Earth-Science Reviews*, 231, 104086. <https://doi.org/10.1016/j.earscirev.2022.104086>
- Korte, C., Hesselbo, S. P., Ullmann, C. V., Dietl, G., Ruhl, M., Schweigert, G., & Thibault, N. (2015). Jurassic climate mode governed by ocean gateway. *Nature Communications*, 6(1), 10015. <https://doi.org/10.1038/ncomms10015>
- Krencker, F.-N., Bodin, S., Suan, G., Heimhofer, U., Kabiri, L., & Immenhauser, A. (2015). Toarcian extreme warmth led to tropical cyclone intensification. *Earth and Planetary Science Letters*, 425, 120–130. <https://doi.org/10.1016/j.epsl.2015.06.003>
- Lanés, S., Manceñido, M. O., & Damborenea, S. E. (2007). Lapispira: A double helicoidal burrow from jurassic marine nearshore environments. In R. G. Bromley, L. A. Buatois, G. Mangan, J. F. Denise, & R. N. Melchor (Eds.), *Sediment-Organism Interactions: A Multifaceted Ichnology* (pp. 59–78). Claremore: SEPM Society for Sedimentary Geology.
- Leanza, H. A., Mazzini, A., Corfu, F., Llambías, E. J., Svensen, H., Planke, S., & Galland, O. (2013). The Chachil Limestone (Pliensbachian–earliest Toarcian) Neuquén Basin, Argentina: U–Pb age calibration and its significance on the Early Jurassic evolution of southwestern Gondwana. *Journal of South American Earth Sciences*, 42, 171–185. <https://doi.org/10.1016/j.jsames.2012.07.012>
- Legarreta, L., & Uliana, M. A. (1996). The Jurassic succession in west-central Argentina: Stratigraphic patterns, sequences and paleogeographic evolution. *Palaeogeography, Palaeoclimatology, Palaeoecology*, 120(3–4), 303–330. [https://doi.org/10.1016/0031-0182\(95\)00042-9](https://doi.org/10.1016/0031-0182(95)00042-9)
- Liu, M., Sun, P., Them, T. R., II, Li, Y., Sun, S., Gao, X., . . . Tang, Y. (2020). Organic geochemistry of a lacustrine shale across the Toarcian Oceanic Anoxic Event (Early Jurassic) from NE China. *Global and Planetary Change*, 191, 103214. <https://doi.org/10.1016/j.gloplacha.2020.103214>
- Manceñido, M. (1990). The succession of Early Jurassic brachiopod faunas from Argentina: Correlations and affinities. In D. I. MacKinnon, D. E. Lee, & J. D. Campbell, J. D. (Eds.), *Brachiopods through Time* (pp. 397–404). Rotterdam: Balkema.

- Mazzini, A., Svensen, H., Lanza, H. A., Corfu, F., & Planke, S. (2010). Early Jurassic shale chemostratigraphy and U–Pb ages from the Neuquén Basin (Argentina): Implications for the Toarcian Oceanic Anoxic event. *Earth and Planetary Science Letters*, 297(3–4), 633–645. <https://doi.org/10.1016/j.epsl.2010.07.017>
- McArthur, J. M., Steuber, T., Page, K. N., & Landman, N. H. (2016). Sr-isotope stratigraphy: Assigning time in the Campanian, Pliensbachian, Toarcian, and Valanginian. *The Journal of Geology*, 124(5), 569–586. <https://doi.org/10.1086/687395>
- McElwain, J. C., Wade-Murphy, J., & Hesselbo, S. P. (2005). Changes in carbon dioxide during an oceanic anoxic event linked to intrusion into Gondwana coals. *Nature*, 435(7041), 479–482. <https://doi.org/10.1038/nature03618>
- Page, K. N. (2003). The Lower Jurassic of Europe: Its subdivision and correlation. *GEUS Bulletin*, 1, 21–59. <https://doi.org/10.34194/geusb.v1.4646>
- Pángaro, F., Melli, A. T., Malone, P., Cevallos, M., Soraci, A., Mosquera, A., & Kim, H. J. (2006). Modelos de entramamiento de la dorsal de Huincul, Cuenca Neuquina, Argentina. *Petrotecnia*, 4, 48–88. <http://biblioteca.iapg.org.ar/ArchivosAdjuntos/Petrotecnia/2006-2/Modelos.pdf>
- Pankhurst, R., Riley, T., Fanning, C., & Kelley, S. (2000). Episodic silicic volcanism in Patagonia and the Antarctic Peninsula: Chronology of magmatism associated with the break-up of Gondwana. *Journal of Petrology*, 41(5), 605–625. <https://doi.org/10.1093/petrology/41.5.605>
- Percival, L. M. E., Witt, M. L. I., Mather, T. A., Hermoso, M., Jenkyns, H. C., Hesselbo, S. P., . . . Ruhl, M. (2015). Globally enhanced mercury deposition during the end-Pliensbachian extinction and Toarcian OAE: A link to the Karoo–Ferrar Large Igneous Province. *Earth and Planetary Science Letters*, 428, 267–280. <https://doi.org/10.1016/j.epsl.2015.06.064>
- Pieńkowski, G., Uchman, A., Ninard, K., Page, K. N., & Hesselbo, S. P. (2024). Early Jurassic extrinsic solar system dynamics versus intrinsic Earth processes – Toarcian sedimentation and benthic life in deep-sea contourite drift facies, Cardigan Bay Basin, UK. *Progress in Earth and Planetary Science*, 11(1), 18. <https://doi.org/10.1186/s40645-024-00612-3>
- Remírez, M. N., & Algeo, T. J. (2020). Carbon-cycle changes during the Toarcian (Early Jurassic) and implications for regional versus global drivers of the Toarcian oceanic anoxic event. *Earth-Science Reviews*, 209, 103283. <https://doi.org/10.1016/j.earscirev.2020.103283>
- Riccardi, A. C. (2008). The marine Jurassic of Argentina: A biostratigraphic framework. *Episodes*, 31(3), 326–335. <https://doi.org/10.18814/epiugs/2008/v31i3/007>
- Ruebsam, W., & Al-Husseini, M. (2020). Calibrating the Early Toarcian (Early Jurassic) with stratigraphic black holes (SBH). *Gondwana Research*, 82, 317–336. <https://doi.org/10.1016/j.gr.2020.01.011>
- Ruebsam, W., & Schwark, L. (2024). Disparity between Toarcian Oceanic Anoxic Event and Toarcian carbon isotope excursion. *International Journal of Earth Sciences*. <https://doi.org/10.1007/s00531-024-02408-8>
- Ruhl, M., Hesselbo, S. P., Jenkyns, H. C., Xu, W., Silva, R. L., Matthews, K. J., . . . Riding, J. B. (2022). Reduced plate motion controlled timing of Early Jurassic Karoo–Ferrar large igneous province volcanism. *Science Advances*, 8(36), eabo0866. <https://doi.org/10.1126/sciadv.abo0866>
- Ruvalcaba Baroni, I., Pohl, A., van Helmond, N. A., Papadomanolaki, N. M., Coe, A. L., Cohen, A. S., . . . Slomp, C. P. (2018). Ocean circulation in the Toarcian (Early Jurassic): A key control on deoxygenation and carbon burial on the European shelf. *Paleoceanography and Paleoclimatology*, 33(9), 994–1012. <https://doi.org/10.1029/2018PA003394>
- Sanei, H., Grasby, S. E., & Beauchamp, B. (2012). Latest Permian mercury anomalies. *Geology*, 40(1), 63–66. <https://doi.org/10.1130/G32596.1>
- Scotese, C. R. (2013). *Paleomap Project*. Retrieved from www.scotese.com
- Silva, R. L., Duarte, L. V., Wach, G. D., Ruhl, M., Sadki, D., Gómez, J. J., . . . Mendonça, J. G. (2021a). An Early Jurassic (Sinemurian-Toarcian) stratigraphic framework for the occurrence of Organic Matter Preservation Intervals (OMPIs). *Earth-Science Reviews*, 221, 103780. <https://doi.org/10.1016/j.earscirev.2021.103780>
- Silva, R. L., Ruhl, M., Barry, C., Reolid, M., & Ruebsam, W. (2021b). Pacing of late Pliensbachian and early Toarcian carbon cycle perturbations and environmental change in the westernmost Tethys (La Cerradura section, Subbetic Zone of the Betic Cordillera, Spain). *Special Publication – Geological Society of London*, 514(1), 387–408. <https://doi.org/10.1144/SP514-2021-27>
- Storm, M. S., Hesselbo, S. P., Jenkyns, H. C., Ruhl, M., Ulmann, C. V., Xu, W., . . . Gorbanenko, O. (2020). Orbital pacing and secular evolution of the Early Jurassic carbon cycle. *Proceedings of the National Academy of Sciences of the United States of America*, 117(8), 3974–3982. <https://doi.org/10.1073/pnas.1912094117>
- Suan, G., Nikitenko, B. L., Rogov, M. A., Baudin, F., Spannberg, J. E., Knyazev, V. G., . . . Lécuyer, C. (2011). Polar record of Early Jurassic massive carbon injection. *Earth and Planetary Science Letters*, 312(1–2), 102–113. <https://doi.org/10.1016/j.epsl.2011.09.050>
- Suan, G., Rulleau, L., Mattioli, E., Suchéras-Marx, B., Rousselle, B., Pittet, B., . . . Föllmi, K. B. (2013). Palaeoenvironmental significance of Toarcian black shales and event deposits from southern Beaujolais, France. *Geological Magazine*, 150(4), 728–742. <https://doi.org/10.1017/S0016756812000970>
- Svensen, H., Planke, S., Chevallier, L., Malthe-Sørensen, A., Corfu, F., & Jamtveit, B. (2007). Hydrothermal venting of greenhouse gases triggering Early Jurassic global warming. *Earth and Planetary Science Letters*, 256(3–4), 554–566. <https://doi.org/10.1016/j.epsl.2007.02.013>
- Svensen, H. H., Jones, M. T., Percival, L. M. E., Grasby, S. E., & Mather, T. A. (2023). Release of mercury during contact metamorphism of shale: Implications for understanding the impacts of large igneous province volca-

- nism. *Earth and Planetary Science Letters*, 619, 118306. <https://doi.org/10.1016/j.epsl.2023.118306>
- Them, T. R., II, Gill, B. C., Caruthers, A. H., Gerhardt, A. M., Gröcke, D. R., Lyons, T. W., . . . Owens, J. D. (2018). Thallium isotopes reveal protracted anoxia during the Toarcian (Early Jurassic) associated with volcanism, carbon burial, and mass extinction. *Proceedings of the National Academy of Sciences of the United States of America*, 115(26), 6596–6601. <https://doi.org/10.1073/pnas.1803478115>
- Them, T. R., II, Jagoe, C. H., Caruthers, A. H., Gill, B. C., Grasby, S. E., Gröcke, D. R., . . . Owens, J. D. (2019). Terrestrial sources as the primary delivery mechanism of mercury to the oceans across the Toarcian Oceanic Anoxic Event (Early Jurassic). *Earth and Planetary Science Letters*, 507, 62–72. <https://doi.org/10.1016/j.epsl.2018.11.029>
- van de Schootbrugge, B., Bailey, T. R., Rosenthal, Y., Katz, M. E., Wright, J. D., Miller, K. G., . . . Falkowski, P. G. (2005). Early Jurassic climate change and the radiation of organic-walled phytoplankton in the Tethys Ocean. *Paleobiology*, 31(1), 73–97. [https://doi.org/10.1666/0094-8373\(2005\)0312.0.CO;2](https://doi.org/10.1666/0094-8373(2005)0312.0.CO;2)
- Vergani, G. D., Tankard, A. J., Belotti, H. J., & Welsink, H. J. (1995). Tectonic evolution and paleogeography of the Neuquén Basin, Argentina. In A. J. Tankard, R. Suárez Soruco, & H. J. Welsink (Eds.), *Petroleum Basins of South America* (pp. 383–402). Boulder: AAPG.
- Vicente, J. C. (2005). Dynamic paleogeography of the Jurassic Andean Basin: Pattern of transgression and localisation of main straits through the magmatic arc. *Revista de la Asociación Geológica Argentina*, 60, 221–250.
- Ware, B., Jourdan, F., & Timms, N. E. (2023). The Ferrar Continental Flood Basalt: A ~1.6 Ma long duration evi-
- denced by high-precision 40Ar/39Ar ages suggest a potential role in the Pliensbachian-Toarcian extinction event. *Earth and Planetary Science Letters*, 622, 118369. <https://doi.org/10.1016/j.epsl.2023.118369>
- Wedepohl, K. H. (1971). Environmental influences on the chemical composition of shales and clays. *Physics and Chemistry of the Earth*, 8, 307–333. [https://doi.org/10.1016/0079-1946\(71\)90020-6](https://doi.org/10.1016/0079-1946(71)90020-6)
- Xu, W., Ruhl, M., Jenkyns, H. C., Hesselbo, S. P., Riding, J. B., Selby, D., . . . Idiz, E. F. (2017). Carbon sequestration in an expanded lake system during the Toarcian oceanic anoxic event. *Nature Geoscience*, 10(2), 129–134. <https://doi.org/10.1038/ngeo2871>
- Xu, W., Mac Niocail, C., Ruhl, M., Jenkyns, H. C., Riding, J. B., & Hesselbo, S. P. (2018a). Magnetostratigraphy of the Toarcian Stage (Lower Jurassic) of the Llanbedr (Mochras Farm) Borehole, Wales: Basis for a global standard and implications for volcanic forcing of palaeoenvironmental change. *Journal of the Geological Society*, 175(4), 594–604. <https://doi.org/10.1144/jgs2017-120>
- Xu, W., Ruhl, M., Jenkyns, H. C., Leng, M. J., Huggett, J. M., Minisini, D., . . . Hesselbo, S. P. (2018b). Evolution of the Toarcian (Early Jurassic) carbon-cycle and global climatic controls on local sedimentary processes (Cardigan Bay Basin, UK). *Earth and Planetary Science Letters*, 484, 396–411. <https://doi.org/10.1016/j.epsl.2017.12.037>

Manuscript received: November 13, 2023

Revision requested: February 05, 2024

Revised version received: March 24, 2024

Accepted: May 28, 2024

The pdf version of this paper includes an electronic supplement

Please save the electronic supplement contained in this pdf-file by clicking the blue frame above. After saving rename the file extension to .zip (for security reasons Adobe does not allow to embed .exe, .zip, .rar etc. files).

Table of contents – Electronic Supplementary Material (ESM)

- Supplementary Fig. 1. Detailed stratigraphic logs
- Supplementary Fig. 2. Detailed chemostratigraphy of the Las Overas 1 composite section
- Supplementary Fig. 3. Invertebrate fauna Arroyo Serrucho
- Supplementary Fig. 4. Invertebrate fauna Las Overas 1 composite section and Las Overas section 2
- Supplementary Plate 1. Photographs of selected key ammonites
- Supplementary data file ($\delta^{13}\text{C}_{\text{TOC}}$, Rock-Eval data, Elemental Data, Mercury)